

The Neonatal Fc Receptor and Complement Fixation Facilitate Prophylactic Vaccine-Mediated Humoral Protection against Viral Infection in the Ocular Mucosa

This information is current as of October 17, 2017.

Derek J. Royer, Meghan M. Carr, Hem R. Gurung, William P. Halford and Daniel J. J. Carr

J Immunol 2017; 199:1898-1911; Prepublished online 31 July 2017;
doi: 10.4049/jimmunol.1700316
<http://www.jimmunol.org/content/199/5/1898>

-
- Supplementary Material** <http://www.jimmunol.org/content/suppl/2017/07/29/jimmunol.1700316.DCSupplemental>
- References** This article **cites 84 articles**, 30 of which you can access for free at:
<http://www.jimmunol.org/content/199/5/1898.full#ref-list-1>
- Subscription** Information about subscribing to *The Journal of Immunology* is online at:
<http://jimmunol.org/subscription>
- Permissions** Submit copyright permission requests at:
<http://www.aai.org/About/Publications/JI/copyright.html>
- Email Alerts** Receive free email-alerts when new articles cite this article. Sign up at:
<http://jimmunol.org/alerts>

The Neonatal Fc Receptor and Complement Fixation Facilitate Prophylactic Vaccine-Mediated Humoral Protection against Viral Infection in the Ocular Mucosa

Derek J. Royer,* Meghan M. Carr,* Hem R. Gurung,[†] William P. Halford,[‡] and Daniel J. J. Carr*[†]

The capacity of licensed vaccines to protect the ocular surface against infection is limited. Common ocular pathogens, such as HSV-1, are increasingly recognized as major contributors to visual morbidity worldwide. Humoral immunity is an essential correlate of protection against HSV-1 pathogenesis and ocular pathology, yet the ability of Ab to protect against HSV-1 is deemed limited due to the slow IgG diffusion rate in the healthy cornea. We show that a live-attenuated HSV-1 vaccine elicits humoral immune responses that are unparalleled by a glycoprotein subunit vaccine vis-à-vis Ab persistence and host protection. The live-attenuated vaccine was used to assess the impact of the immunization route on vaccine efficacy. The hierarchical rankings of primary immunization route with respect to efficacy were s.c. \geq mucosal $>$ i.m. Prime-boost vaccination via sequential s.c. and i.m. administration yielded greater efficacy than any other primary immunization route alone. Moreover, our data support a role for complement in prophylactic protection, as evidenced by intracellular deposition of C3d in the corneal epithelium of vaccinated animals following challenge and delayed viral clearance in C3-deficient mice. We also identify that the neonatal Fc receptor (FcRn) is upregulated in the cornea following infection or injury concomitant with increased Ab perfusion. Lastly, selective small interfering RNA-mediated knockdown of FcRn in the cornea impeded protection against ocular HSV-1 challenge in vaccinated mice. Collectively, these findings establish a novel mechanism of humoral protection in the eye involving FcRn and may facilitate vaccine and therapeutic development for other ocular surface diseases. *The Journal of Immunology*, 2017, 199: 1898–1911.

The mechanisms by which systemic vaccination strategies induce protective immunity against various mucosal pathogens are incompletely understood. However, the ability of systemic vaccines to protect against mucosal pathogen-associated diseases is contingent on vaccine composition, immunization route, and degree of immunologic or anatomic tissue compartmentalization (1–3). Direct mucosal vaccination as an alternative means to elicit site-specific protection is an area of active research (4). Accordingly, some investigators have suggested that immune responses elicited from systemic vaccination may not faithfully recapitulate protective immune responses generated in a mucosal microenvironment (5). However, in the ocular surface mucosae, robust local immune responses to infection are often detrimental. Even transient inflammatory events in the eye can provoke devastating consequences resulting in permanent vision loss. Therefore, the ocular surface mucosa presents additional complexity to the equation of systemic vaccination.

The cornea is unique among immune-privileged tissues because of its direct exposure to the external environment. However, the cornea remains vulnerable to immune-mediated pathological sequelae resulting from injury, toxicity, or infection. These vision-altering sequelae include scarring, neovascularization, and desiccation. Moreover, select pathogens representing essentially every taxonomic classification ranging from bacteria and viruses to yeast, protozoa, and nematodes are associated with infections of the ocular surface mucosae (6). The global burden of infectious external eye disease is formidable in terms of visual morbidity (7). Despite this, no licensed vaccine capable of preventing a single ocular surface infection exists, excluding varicella zoster virus.

Concern remains that boosting immunity by way of vaccination against a common ocular pathogen, such as HSV-1, may exacerbate the severity of ocular pathology (8). Although the global incidence of HSV-1 keratitis is estimated at 1.5 million new cases annually, its economic burden in the United States alone is projected to exceed \$23 million in treatment-associated costs in 2017 (9, 10). Treatment cost projection is based upon consumer price index inflation calculations reported by the U.S. Bureau of Labor

*Department of Ophthalmology, University of Oklahoma Health Sciences Center, Oklahoma City, OK 73104; [†]Department of Microbiology and Immunology, University of Oklahoma Health Sciences Center, Oklahoma City, OK 73104; and [‡]Department of Medical Microbiology, Immunology, and Cell Biology, Southern Illinois University School of Medicine, Springfield, IL 62794

ORCID: 0000-0002-8476-1784 (D.J.R.); 0000-0003-1954-2478 (D.J.J.C.).

Received for publication February 28, 2017. Accepted for publication July 3, 2017.

This work was supported by National Institutes of Health Grants R01 EY021238, P30 EY021725, and T32 EY023202. Additional support was provided by an unrestricted grant from Research to Prevent Blindness. Funding for Imaris software was provided by a grant from the Presbyterian Health Foundation.

D.J.R. designed and conducted experiments, analyzed data, and prepared the manuscript; H.R.G. acquired confocal images in Fig. 5C; M.M.C. assisted with vaccinating animals, tissue processing, and image quantification; W.P.H. designed the HSV-1 0ΔNLS virus and critiqued the manuscript; and D.J.J.C. conducted experiments and supervised all work.

The content of the manuscript is solely the responsibility of the authors and does not necessarily represent the official views of the National Institutes of Health or the National Eye Institute.

Address correspondence and reprint requests to Dr. Daniel J.J. Carr, Department of Ophthalmology, University of Oklahoma Health Sciences Center, Dean McGee Eye Institute, Room 415A, 608 Stanton L. Young Boulevard, Oklahoma City, OK 73104. E-mail address: Dan-Carr@ouhsc.edu

The online version of this article contains supplemental material.

Abbreviations used in this article: ADCC, Ab-dependent cell cytotoxicity; EpCAM, epithelial cell adhesion molecule; FcRn, neonatal Fc receptor; FMO, fluorescence minus one; LAT, latency-associated transcript; MFI, median fluorescence intensity; MLN, mandibular lymph node; NLS, nuclear localization sequence; PI, postinfection; SD-OCT, spectral domain optical coherence tomography; siRNA, small interfering RNA; TG, trigeminal ganglia; WT, wild-type.

Copyright © 2017 by The American Association of Immunologists, Inc. 0022-1767/17/\$30.00

Statistics (https://www.bls.gov/data/inflation_calculator.htm) relative to the original cost estimate reported in 2003 by Lairson et al. (10). Many experimental strategies and approaches have been applied in the preclinical development of prophylactic HSV-1 vaccines, with a specific focus on preventing ocular disease (11–17). However, our recent findings comprehensively established that humoral immunity is a strong correlate of protection against HSV-1 pathogenesis and resultant ocular disease in mice using a live-attenuated vaccine that is avirulent and highly immunogenic due to deletion of the nuclear localization sequence (NLS) in the ICPO gene (17, 18). This vaccine is designated HSV-1 0ΔNLS (17). Prophylactic vaccine-induced HSV-specific serum Ab concentration is also recognized as a major correlate of protection against HSV-1-associated disease in humans (19).

Efficient humoral protection against mucosal infections requires a sufficient amount of pathogen-specific Ab at the site of infection to counter replication and dissemination (20). Avascular tissues, such as the cornea, contain drastically less Ig during homeostatic conditions compared with other mucosal sites, although an upsurge in the concentration of IgG has been reported in the cornea and tear film during microbial keratitis (20–22). Although humoral immunity is a major correlate of protection against HSV-1 pathogenesis and tissue pathology (17), the mechanism facilitating humoral protection in the cornea remains vague. In this article, we explore the dynamics and mechanisms of prophylactic vaccine-mediated humoral protection against HSV-1 in the eye. First, we distinguish that the longevity of humoral protection elicited by a glycoprotein D subunit vaccine (glycoprotein D-2) is short-lived in mice compared with the recently characterized live-attenuated HSV-1 0ΔNLS vaccine (17, 18). We compare various routes of immunization and identify that the efficacy of the HSV-1 0ΔNLS vaccine is limited following classical i.m. injection alone. Furthermore, our data support a role for complement fixation in prophylactic protection, as evidenced by intracellular deposition of C3d in the corneas of vaccinated animals following ocular HSV-1 challenge. This finding was corroborated by delayed viral clearance in vaccinated C3-deficient animals relative to wild-type (WT) upon ocular challenge. We also investigate the dynamics of Ab perfusion in the corneas of immunologically naive mice during HSV-1 infection and uncover a novel role for the neonatal Fc receptor (FcRn) in regulating Ab transcytosis and host defense in the corneal epithelium. Although FcRn was first characterized for its role in transferring IgG from a mother's milk across the gut lumen in neonates, it plays many other important roles involving IgG transport and turnover across the lifespan (23). We anticipate that these findings will influence future vaccination strategies targeted against mucosal pathogens at the ocular surface.

Materials and Methods

Mice

Male and female outbred CD-1 mice were purchased from Charles River Laboratories (Wilmington, MA). The rationale for using an outbred mouse line for a majority of this vaccine study focuses on the genetic heterozygosity and immunologic diversity of CD-1 mice relative to C57BL/6 (24). Outbred "Swiss" mice, such as the CD-1 stock, are also more susceptible to HSV-1 neuropathogenesis than C57BL/6 mice (25). However, inbred C57BL/6 WT, complement C3-deficient (C3^{-/-}), and FcγRIII-deficient (FcγRIII^{-/-}) mice were obtained from the Jackson Laboratory (Bar Harbor, ME) to clarify immunologic mechanisms of Ab-mediated protection. Animals were housed in a specific pathogen-free vivarium at the Dean McGee Eye Institute on the University of Oklahoma Health Sciences Center. Investigators adhered to procedures approved by the University of Oklahoma Health Sciences Center Institutional Animal Care and Use Committee (Protocol # 16-087-SSIC-A), and animals were handled in accordance with the National Institutes of Health's *Guide for the Care and Use of Laboratory Animals*. Animals were anesthetized for all procedures

using an i.p. injection of ketamine (100 mg/kg) and xylazine (6.6 mg/kg). For terminal experiments requiring tissue collection, mice were anesthetized and euthanized by exsanguination via intracardiac perfusion with 10 ml of PBS.

Vaccines, immunization schemes, and ocular infection

The HSV-1 0ΔNLS vaccine was used for immunization, with each dose consisting of 5×10^4 PFU, as described previously (17). Briefly, each dose of the glycoprotein D-2 subunit vaccine included 2.5 μg of glycoprotein D-2 protein adjuvanted with 25 μl of Injectal alum (Thermo Fisher Scientific, Waltham, MA) and 10 μg of monophosphoryl lipid A from *Salmonella* (Sigma-Aldrich, St. Louis, MO). The glycoprotein D-2 protein is a truncated form of HSV-2 glycoprotein D and was generated and purified as described previously (26). This formulation has been used previously in animal models to mimic the GlaxoSmithKline Herpevac vaccine, which was 82% effective against HSV-1-associated genital disease in clinical trials (17, 19, 26). The glycoprotein D-2 vaccine was used as a control in these studies, because the HSV-2 glycoprotein D immunogen elicits cross-protective neutralizing Ab responses against HSV-1 glycoprotein D (27). Animals were vaccinated using a two-dose prime-boost regimen in the footpad and flank, respectively, with the live-attenuated HSV-1 0ΔNLS or glycoprotein D-2 subunit vaccine, as previously described (17). The booster vaccination was given 3 wk after the primary vaccination. To evaluate the effect of the vaccination route on efficacy, animals were vaccinated in the hind footpad alone (s.c.), in the hind flank alone (i.m.), by single intranasal inoculation (mucosal), or with a footpad-flank boost combination regimen as a positive control.

Outbred CD-1 mice were infected by applying 1×10^3 PFU HSV-1 McKrae to each cornea following partial epithelial debridement with a 25-gauge needle at the times indicated in each figure legend. Inbred C57BL/6 mice were infected with 1×10^4 PFU HSV-1 McKrae per eye. Vaccinated animals were challenged 7 wk after the primary vaccination, unless indicated otherwise. When necessary, animals were subjected to partial epithelial debridement as a scratch-only mock-infection control.

Serological and virological assays

Peripheral blood was collected from the facial vein of anesthetized mice at the specified times postvaccination or challenge and fractionated using Microtainer serum separation tubes (Becton Dickinson, Franklin Lakes, NJ). Serum titers were assessed for virus-neutralizing titers in the presence of guinea pig complement (Rockland, Limerick, PA) on confluent Vero cells (American Type Culture Collection, Manassas, VA), as previously described (17). Virus-specific Ab subclass profiling was quantified by ELISA using immobilized HSV-1 virions as a target and alkaline phosphatase-conjugated anti-mouse Ig subclass-specific detection Abs (SouthernBiotech, Birmingham, AL), as described (18). To quantify titers of infectious virus, corneas were swabbed with cotton-tipped applicators to collect free virus shed in the tear film, and tissues were excised for downstream analysis by standard plaque assay on Vero cells (17). For detection of latent virus, RNA was extracted from cornea-innervating trigeminal ganglia (TG) harvested from mice at day 30 postinfection (PI), RNA was converted into cDNA, and viral transcript expression was evaluated by PCR relative to β-actin expression and normalized to uninfected control samples, as previously described (17). Alternatively, direct quantification of viral genome copy number was performed by PCR on DNA isolated from the TG of challenged mice using a proprietary primer-probe mix, according to the manufacturer's directions (Primerdesign, Chandler's Ford, U.K.), as described (18).

Spectral domain optical coherence tomography

Noninvasive in vivo imaging of the anterior segment was performed on anesthetized animals using a Bioptigen spectral domain optical coherence tomography (SD-OCT) system (Leica Microsystems, Triangle Park, NC) to assess corneal structure and inflammation, as previously characterized (28, 29).

Immunohistochemistry and confocal microscopy

Corneas were cut from enucleated eyes of euthanized animals, fixed in a 4% solution of paraformaldehyde (Sigma-Aldrich) for 30 min, and washed in $1 \times$ PBS containing 1% Triton X-100. Corneas were blocked using anti-CD16/32 Fc block overnight (eBioscience, San Diego, CA) and immunolabeled, as described previously, to quantify corneal neovascularization (30). Phalloidin (Life Technologies, Carlsbad, CA) and DAPI staining were used to identify tissue layers and boundaries. Mast cell granules were stained with FITC-avidin, as described (31). Unconjugated goat anti-mouse C3d (cat. no. AF2655) and goat anti-mouse FcRn (cat. no. AF6775; both from R&D Systems, Minneapolis, MN) primary Abs were

used to label each respective protein in the cornea. Dako polyclonal rabbit anti-HSV-1 Ab was used for viral Ag detection (Agilent Technologies, Santa Clara, CA). Appropriate fluorochrome-conjugated secondary Abs were used for confocal imaging (Jackson ImmunoResearch, West Grove, PA). Images were acquired using an Olympus FV1200 confocal microscope in sequential channel scanning mode (Center Valley, PA). Three-dimensional protein fluorescence colocalization analysis was performed using Imaris software (Bitplane, Concord, MA).

Quantification of tissue Ab concentrations

Corneas and TG from healthy, cornea-scratch control (24 h postinjury), and HSV-1-infected (24 and 48 h PI) mice were collected along with ear pinna specimens from healthy or ear-punched mice (24 h postinjury). Samples were placed in Next Advance GREEN bead lysis tubes (Averill Park, NY) containing 150 μ l of radioimmunoprecipitation assay lysis buffer supplied with protease inhibitor (Santa Cruz Biotechnology, Dallas, TX), homogenized in a Next Advance Bullet Blender Storm 24 homogenizer for 10 min, and subjected to sonication in a water bath for 10 min. Supernatants were clarified by centrifugation at 16,000 \times g for 10 min and used for downstream analysis. Tissue supernatants were surveyed for Ab content using a mouse Ab isotyping multiplex kit (eBioscience) on a Bio-Plex system (Bio-Rad, Hercules, CA), according to the manufacturers' directions. Data are reported as picogram of Ig isotype per milligram tissue wet weight.

Flow cytometry

Single-cell suspensions were generated from all tissue collected for analysis by flow cytometry. Briefly, lymph nodes were macerated over 40- μ m mesh to generate a suspension. Individual corneas were digested in 0.25 Wünsch units of Liberase TL enzyme mix (Roche Diagnostics, Indianapolis, IN), suspended in 500 μ l of RPMI 1640 media supplemented with 10% heat-inactivated FBS, gentamicin, and antibiotic/antimycotic (Invitrogen, Carlsbad, CA) at 37°C for 2 h, and exposed to mechanical trituration every 20 min. Corneal digests were filtered through 40- μ m mesh prior to labeling. Peripheral blood was collected from the facial vein, and erythrocytes were removed through two incubations in hypotonic lysing buffer, as described (32). Cell suspensions were blocked with anti-CD16/32 (eBioscience), labeled with target-specific Abs for 20–30 min, and washed in 1 \times PBS containing 1% BSA.

Intracellular FcRn labeling was performed with an unlabeled primary Ab (R&D Systems) and a fluorochrome-conjugated secondary Ab (Jackson ImmunoResearch) using a saponin-based Perm/Wash Buffer (BD Biosciences, San Jose, CA). All samples were analyzed on a MACSQuant 10 flow cytometer with MACSQuantify software (both from Miltenyi Biotec, Bergisch Gladbach, Germany). Gating boundaries were established via isotype labeling and/or fluorescence minus one (FMO) controls to ensure Ab specificity and negate spectral overlap, respectively. Biological negative controls were also considered. Gating strategies are shown within this article or are based on those published previously (17, 31, 33).

Western blot

Supernatants from healthy or HSV-1-infected cornea homogenates were prepared in radioimmunoprecipitation assay buffer, as described above. Sample protein concentrations were standardized using a Pierce BCA protein assay kit (Thermo Fisher Scientific). Proteins were resolved by electrophoresis on Novex Tris-glycine 4–20% gradient polyacrylamide gels (Invitrogen) and transferred onto nitrocellulose membranes. Membranes were blocked for 1 h at room temperature in 5% BSA (Sigma-Aldrich) in Tris-buffered saline containing 0.2% Tween 20. Blots were incubated overnight at 4°C in goat anti-mouse FcRn Ab (cat. no. AF6775; 1:2000 dilution; R&D Systems) or for 90 min at room temperature in mouse anti-mouse β -actin primary Ab (cat. no. ab6276; 1:10,000 dilution; Abcam, Cambridge, MA). Blots were subsequently incubated with the corresponding HRP-conjugated anti-mouse secondary Ab for FcRn (HRP anti-goat; 1:5000 dilution; R&D Systems) or β -actin (HRP anti-mouse; 1:4000 dilution; Amersham, GE Healthcare Bio-Sciences, Pittsburgh, PA) for 1 h at room temperature and imaged using a Kodak in vivo imaging system F Pro (Rochester, NY) with MI SE version 4.4 software (Carestream Health, Rochester, NY). Chemiluminescent detection was achieved using SuperSignal extended duration substrate (Thermo Fisher Scientific). Band intensity analysis was performed using ImageJ (National Institutes of Health, Bethesda, MD).

Small interfering RNA transfection

For corneal FcRn-knockdown experiments, Ambion Silencer Select siRNA (Invitrogen) was used, as previously described, with Lipofectamine

RNAiMAX (Invitrogen) transfection reagent (33). Briefly, the apical corneal epithelium was partially debrided to facilitate efficient transfection, and a drop containing 5 μ l of Lipofectamine and 3.33 nmol FcRn-specific or nonspecific scramble control small interfering RNAs (siRNAs) in supplement-free DMEM was applied to each cornea. siRNA sequences were designed and validated by the manufacturer, although FcRn was targeted with two nonoverlapping siRNAs to enhance effectiveness (Supplemental Table I). Knockdown efficiency was confirmed by Western blot.

Statistical analysis

Prism 5 software (GraphPad, San Diego, CA) was used for statistical analysis. Data reflect mean \pm SEM unless indicated otherwise. The statistical tests used for analysis are described in each figure legend. Significance thresholds for comparisons are denoted as follows: * p < 0.05, ** p < 0.01, *** p < 0.001.

Results

Humoral protection elicited by a glycoprotein D-2 subunit vaccine is short-lived compared with the live-attenuated HSV-1 Δ NLS vaccine

Clinical trials for HSV vaccines have favored subunit vaccines over live-attenuated viruses, with limited success reported to date (8). Evidence from the GlaxoSmithKline Herpevac clinical trials using a glycoprotein D subunit vaccine from HSV-2 demonstrated that glycoprotein D-2-reactive Abs exhibit moderate cross-protection against HSV-1 (19, 27). Therefore, we previously used a similar glycoprotein D-2 subunit vaccine as a measure of comparison for the efficacy of HSV-1 Δ NLS against ocular challenge in CD-1 mice (17). That study unequivocally demonstrated that HSV-1 Δ NLS was superior to a glycoprotein D-2 subunit vaccine in its capacity to elicit high-titer neutralizing Ab responses and prevent ocular pathology, but animals were challenged merely 1 mo after vaccination (17). To assess the longevity of prophylactic vaccine-mediated humoral protection comparing HSV-1 Δ NLS with a glycoprotein D-2 subunit, CD-1 mice were vaccinated s.c. in the footpad, given an i.m. booster dose in the ipsilateral flank 21 d later, and subjected to blood collection at 30-d intervals over 3 mo for serology (Fig. 1A).

Mean serum titers of HSV-1-specific Ab were quantified by ELISA on immobilized virions at day 90 postboost (Fig. 1B). Serum titers of HSV-1-specific IgG1, IgG2a, and IgG2b fell below the limit of detection at day 90 postboost in glycoprotein D-2-immunized animals (Fig. 1B). In contrast, HSV-1-specific Ab titers were detected in all mice immunized with HSV-1 Δ NLS, with a predominant IgG1 response (Fig. 1B). Serum titers of HSV-1-specific IgA and IgM were not detected in either group. Virus-neutralization titers were also evaluated in sera collected serially at days 30, 60, and 90 postboost. As previously demonstrated (17), by day 30 postboost, mice immunized with HSV-1 Δ NLS acquire higher virus-neutralizing serum titers than mice immunized with glycoprotein D-2 (Fig. 1C). However, the serum-neutralizing capacity of animals immunized with glycoprotein D-2 was short-lived and declined nearly to the limit of detection (1:25) by day 90 postboost (Fig. 1C). A modest longitudinal decrease from the peak serum neutralization titer was also observed in HSV-1 Δ NLS-vaccinated mice, but the titers at days 60 and 90 postboost remained substantially higher than even the peak titer measured in glycoprotein D-2-vaccinated animals (Fig. 1C). Collectively, our data show that the live-attenuated HSV-1 Δ NLS vaccine elicits a sustained high-titer neutralizing Ab response that is unparalleled by a subunit vaccine, as reported for other common vaccines (34).

Vaccinated animals were subsequently subjected to a deferred challenge at day 90 postboost to investigate whether the discrepancy in Ab titers between mice immunized with HSV-1 Δ NLS and the glycoprotein D-2 subunit had an appreciable impact on vaccine efficacy (Fig. 1A). Animals were challenged bilaterally with an inoculum of 1×10^3 PFU HSV-1 McKrae per eye. Survival

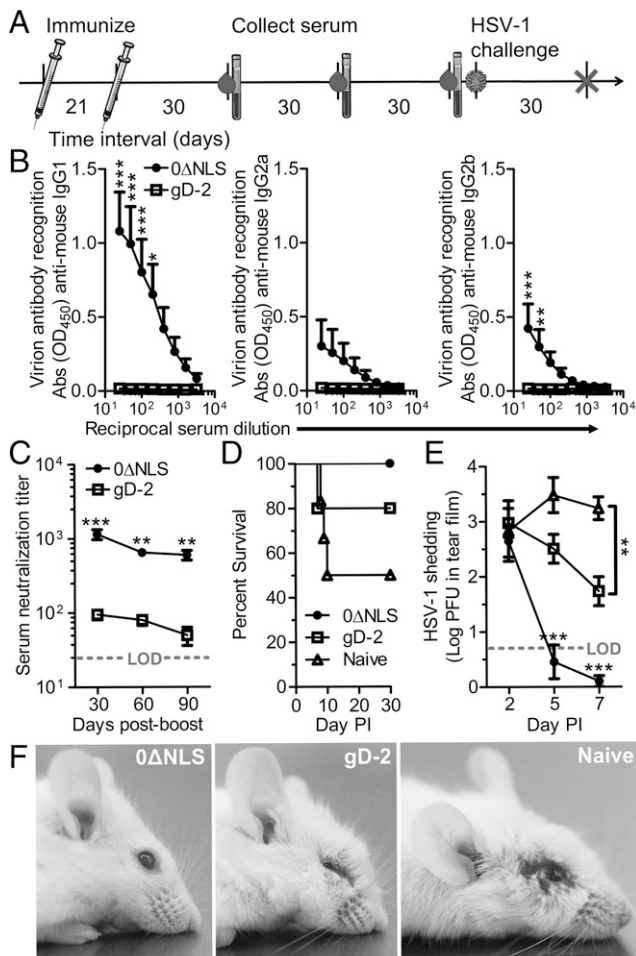


FIGURE 1. Longevity and efficacy of vaccine-induced humoral immune responses comparing subunit and live-attenuated HSV-1 vaccines. **(A)** Experimental timeline detailing vaccination scheme, serial blood draws, and ocular HSV-1 infection. Animals were immunized s.c. with HSV-1 0ΔNLS or a glycoprotein D-2 subunit vaccine, followed by an i.m. boost 3 wk later. Blood was collected every 30 d to assess the humoral immune response to HSV-1. Animals were challenged with 1000 PFU HSV-1 McKrae per eye 90 d following the final immunization. **(B)** ELISA-based characterization of Ig subtypes binding to immobilized HSV-1 virions, including IgG1, IgG2a, and IgG2b, in mouse serum collected at day 90 postboost. Serum samples were diluted on a 2-fold dilution series from 1:25 to 1:3200. HSV-specific IgA and IgM were below the limit of detection. **(C)** HSV-1–neutralization titers recorded from sera taken at days 30, 60, and 90 postboost. **(D)** Animal survival following ocular infection with 1000 PFU HSV-1 McKrae. **(E)** Time course of HSV-1 shedding in the tear film of ocularly infected mice, as determined by plaque assay. **(F)** Representative photographs of mice at 8 d PI. Mice vaccinated with HSV-1 0ΔNLS maintained a healthy appearance, whereas mice vaccinated with the glycoprotein D-2 subunit developed periocular edema and head swelling. Naive mice developed viral lesions in the periocular skin in addition to head swelling. Data in (B)–(E) reflect mean ± SEM for five or six mice per group with two independent experiments. (A) was prepared using Servier Medical Art (www.servier.com) via Creative Commons 3.0. ***p* < 0.01, ****p* < 0.001, HSV-1 0ΔNLS versus glycoprotein D-2 vaccine, unless indicated otherwise, two-way ANOVA with the Bonferroni multiple-comparisons test.

proportions for CD-1 mice infected 90 d following the boost vaccination were three of six naive, four of five glycoprotein D-2 vaccinated, and six of six HSV-1 0ΔNLS vaccinated (Fig. 1D). Acute viral shedding in the tear film was equal among all groups at day 2 PI, but it dropped precipitously in animals vaccinated with HSV-1 0ΔNLS by day 5 PI (Fig. 1E). Although glycoprotein D-2 subunit-vaccinated animals exhibited less viral shedding than naive animals

by day 7 PI (Fig. 1E), they were not spared from developing periocular edema or hydrocephalus (Fig. 1F), a pathognomonic sign of viral encephalitis. Likewise, naive animals developed edematous periocular lesions and hydrocephalus by day 8 PI (Fig. 1F).

Animals infected at day 90 postboost were subsequently assessed for latent viral burden, serology, and tissue pathology at day 30 PI. Although glycoprotein D-2 subunit–vaccinated animals had less latent virus in the TG than naive animals, prophylactic vaccination with HSV-1 0ΔNLS diminished the establishment of viral latency in the TG after ocular challenge (Fig. 2A). Serum-neutralizing titers for HSV-1 were equivalent among all experimental groups by day 30 PI (Fig. 2B), indicating that the humoral immune response to HSV-1 is not directly governed by the quantity or persistence of viral Ag. Moreover, these levels were similar to serum titers observed in HSV-1 0ΔNLS–vaccinated animals at day 30 postboost (Fig. 1C).

The extent of corneal pathology following ocular challenge was evaluated by assessing corneal sensation, neovascularization, and structural integrity. Corneal sensation loss is a highly sensitive pathological outcome of ocular HSV-1 infection and is useful as a measurement of vaccine efficacy against HSV-associated ocular disease (35, 36). Corneal sensation was preserved in HSV-1 0ΔNLS–vaccinated mice, partially lost in glycoprotein D-2–immunized mice, and severely diminished in naive mice at day 30 PI (Fig. 2C). Corneal neovascularization is another vaccine-preventable outcome of herpetic keratitis (17). Neovascularization was evaluated by immunolabeling CD31 and Lyve-1 to visualize corneal blood and lymphatic vessels, respectively. The corneas of animals vaccinated with HSV-1 0ΔNLS remained avascular at day 30 PI (Fig. 2D); however, corneal neovascularization was moderate in glycoprotein D-2–vaccinated animals and severe in naive animals, such that the vessels covered the entire cornea (Fig. 2D).

SD-OCT was used to assess the structural integrity of the anterior eye in vivo at day 30 PI. Corneal SD-OCT imaging in mice immunized with HSV-1 0ΔNLS revealed healthy optically clear corneas with normal light reflexes (Fig. 2E, upper left panel), although a pronounced hyperintensity consistent with leukocyte infiltrate was observed in the central corneas (Fig. 2E, lower left panel). In contrast, corneas of mice immunized with glycoprotein D-2 exhibited moderate corneal opacity (Fig. 2E, upper middle panel), consistent with alterations in the corneal structure (Fig. 2E, lower middle panel). Cellular infiltrate was also observed in the lens of glycoprotein D-2–immunized mice (Fig. 2E, lower middle panel). Moreover, postinfectious mydriasis (dilated pupil) was observed in half of the eyes of glycoprotein D-2–immunized mice (Fig. 2E, middle panels). Stark corneal opacity (Fig. 2E, upper right panel) and lens infiltrate (Fig. 2E, lower right panel) were detected in the eyes of naive animals. In contrast to the other groups, adhesions formed between the iris and cornea and/or iris and lens (designated clinically as anterior and posterior synechia, respectively) of naive animals (Fig. 2E, lower right panel). Postinfectious mydriasis and development of iris adhesions are consistent with the development of anterior uveitis during acute HSV-1 infection (37). Taken together, the data confirm our previous finding that the HSV-1 0ΔNLS vaccine is superior to a glycoprotein D-2 subunit in terms of enabling acute viral clearance, limiting latent infection, and preventing ocular pathology (17). However, data from this study using a delayed challenge model show that the humoral immune response elicited by HSV-1 0ΔNLS sustains its protective effect over time, whereas humoral immunity elicited by glycoprotein D-2 subunit vaccination wanes quickly.

Routes of immunization influence IgG subclass profiles and vaccine efficacy

Routes of immunization are known to distinctively influence vaccine responsiveness, despite the routine clinical use of i.m.

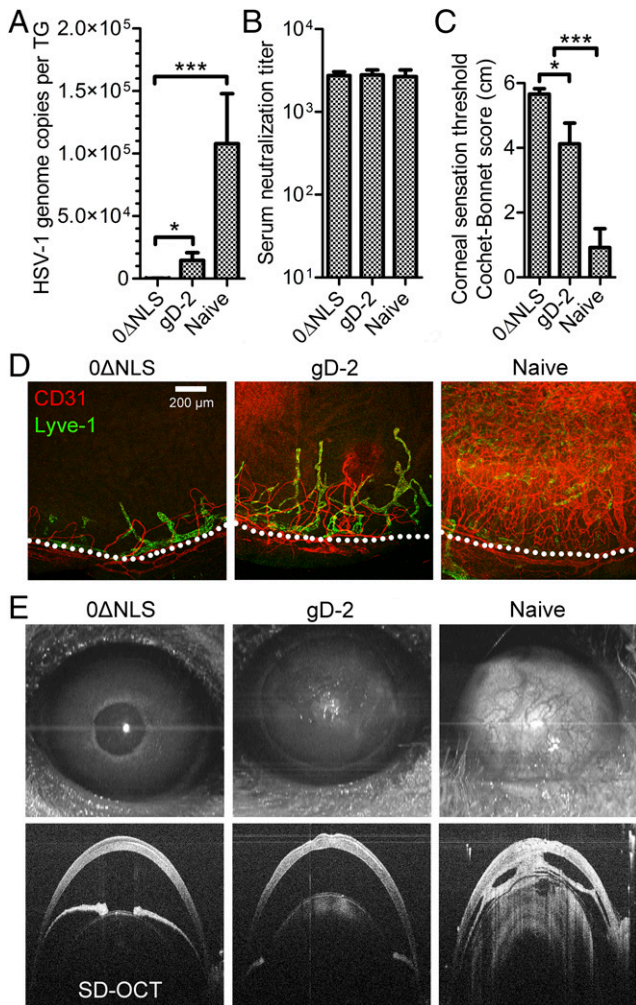


FIGURE 2. HSV-1 0ΔNLS induces lasting protection that prevents ocular pathology upon challenge. Mice ocularly challenged with HSV-1 at 90 d postvaccination, as depicted in Fig. 1A, were evaluated for latent virus, serostatus, and tissue pathology at day 30 PI. (A) Quantitative PCR analysis of HSV-1 genome copy number in the TG. (B) Serum-neutralization titers recorded at day 30 PI. (C) Assessment of corneal sensation in vaccinated or naive mice surviving at day 30 PI using standard Cochet-Bonnet esthesiometry scoring. (D) Representative confocal images of corneal neovascularization in vaccinated and naive mice depicting CD31⁺ blood vessels (red) and Lyve-1⁺ lymphatic vessels (green). Dotted lines represent the anatomic limbal vessels circumscribing the normally avascular cornea. (E) Representative anterior projection of SD-OCT images highlighting the cornea at day 30 PI in HSV-1 0ΔNLS- or glycoprotein D-2-immunized mice or naive mice. Data in (A)–(C) reflect mean ± SEM for three to six mice per group (6–12 corneas or total TG) with two independent experiments. Images in (D) and (E) are representative of five to nine corneas per group. **p* < 0.05, ****p* < 0.001, one-way ANOVA using the Student–Newman–Keuls multiple-comparisons test.

injection. Mice were immunized with HSV-1 0ΔNLS in various sites to assess how unique tissue microenvironments impact immunogenicity and efficacy. Intramuscular, mucosal, and s.c. routes of immunization were modeled by administering equivalent titers of HSV-1 0ΔNLS in the hind leg flank, intranasally, or in the footpad of CD-1 mice, respectively. Postvaccination serum-neutralizing Ab titers were lowest in the flank-only immunization group and were similar between intranasal and footpad vaccination groups, but no single vaccination site generated as strong of a neutralizing Ab response as was observed using a dual prime-boost immunization strategy in the footpad and flank (Fig. 3A).

Flank-only vaccination elicited the highest titers of HSV-specific IgG1 (Fig. 3B), despite the reduced virus-neutralization capacity in this group (Fig. 3A). The HSV-specific IgG1 response was negligible following footpad-only vaccination (Fig. 3B). All routes of vaccination elicited IgG2a (Fig. 3C) and IgG2b (Fig. 3D) responses, but titers were not statistically different among groups following primary vaccination alone.

The route of immunization had a clear impact on the efficacy of protection following HSV-1 challenge. It was suspected that intranasal vaccination could have an advantage for ocular protection relative to the other sites by establishing a population of tissue-resident memory CD8⁺ T cells within the cornea-innervating TG. However, no increase in the number of CD69⁺ CD103⁺ CD8⁺ T cells was observed in TG from intranasally immunized mice at 30 d postvaccination relative to healthy nonvaccinated controls (data not shown). Viral shedding in the ocular tear film was sustained for a longer period of time in mice immunized in the flank only (i.m.) relative to other vaccination sites (Fig. 4A). However, virus was largely cleared from the corneas of all vaccinated mice by day 7 PI (Fig. 4B). A higher tendency toward viral trafficking to the TG and brainstem was observed in mice immunized in the flank or intranasally relative to the other sites in which neurodissemination was absent (Fig. 4B). Trends in delayed viral clearance in the cornea or nervous system (Fig. 4B) correlated with amplified adaptive immune responses in the cornea-draining mandibular lymph nodes (MLNs) at day 7 PI (Fig. 4C, 4D). Therefore, the lack of lymphocyte expansion in the MLNs upon ocular challenge is a useful prognostic correlate of vaccine efficacy in terms of acute viral clearance, as reported previously (17).

Efficient viral clearance is a goal of prophylactic HSV-1 vaccination, but the ultimate measure of vaccine efficacy is its ability to reduce the amount of latent virus in the TG and prevent ocular disease. All routes of immunization reduced the total amount of latent HSV-1 in the TG, as assessed by latency-associated transcript (LAT) RNA expression levels (Fig. 5A), relative to levels previously reported in naive control CD-1 mice infected with a 200-PFU challenge inoculum (17). However, animals that received the two-dose prime-boost vaccination had the lowest levels of latent HSV-1 in the TG after a high-titer ocular 1×10^3 -PFU challenge in terms of LAT expression and viral genome copy number (Fig. 5A, 5B).

Corneas of immunized and challenged mice were evaluated for corneal neovascularization at day 30 PI. Corneas from mice vaccinated intranasally or by prime-boost footpad–flank vaccination maintained a healthy avascular appearance (Fig. 5C–E). Although mice vaccinated in the footpad alone were spared from corneal hemangiogenesis (Fig. 5D), corneal lymphangiogenesis was observed (Fig. 5E). Mice vaccinated in the flank only developed moderate corneal neovascularization involving lymphangiogenesis and hemangiogenesis (Fig. 5C–E). Lastly, the number of leukocytes in the corneas of each group was assessed at day 30 PI (Fig. 5F). No differences in cell numbers were observed that correlated with the tissue neovascularization status aside from a tendency toward elevated numbers of CD45⁺ leukocytes within vascularized corneas (Fig. 5F). Based on acute viral clearance, viral latency, and ocular pathology data, it is apparent that i.m. vaccination alone is not suitable for eliciting the full protective efficacy of the HSV-1 0ΔNLS vaccine.

Ab biodistribution and effector function in herpetic keratitis

Paracellular diffusion of large macromolecules, including Igs and many therapeutic drugs, is restricted in the cornea under homeostatic conditions because of the densely organized tissue architecture and physiological mechanisms that maintain transparency

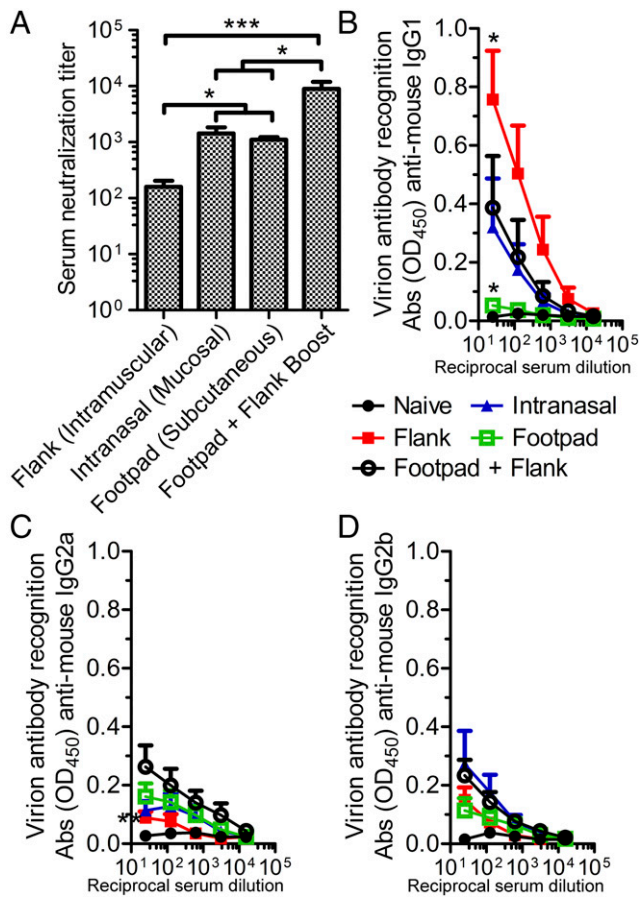


FIGURE 3. Immunization route impacts the humoral response to HSV-1 0ΔNLS. Mice were vaccinated with 5×10^4 PFU HSV-1 0ΔNLS in the flank, footpad, or intranasally using a primary immunization only. Mice receiving a combined footpad vaccination, followed by a flank-boost vaccination 3 wk later, were used as a control. Serum was collected from animals 7 wk after the primary immunization to assess virus-neutralization titers (A) or IgG isotype recognition of HSV-1 by ELISA (B–D). All data reflect mean \pm SEM with three or four independent experiments; $n = 11$ mice per group in (A); $n = 7$ or 8 mice per vaccinated group and $n = 4$ naive mice per group in (B)–(D). * $p < 0.05$, ** $p < 0.01$, *** $p < 0.001$ versus the mean value of the footpad + flank boost group, unless indicated otherwise, nonparametric Kruskal–Wallis test with the Dunn multiple-comparisons tests (A), two-way ANOVA with the Bonferroni multiple-comparisons test (B–D).

(38–40). However, the dynamics of humoral immunity in the cornea during inflammation or infection is not well characterized. To address Ab biodistribution in inflamed corneas, we measured Ig concentrations using a bead-based multiplex array in tissue homogenates from immunologically naive CD-1 mice following infection or mock infection. Concentrations of virtually all Ig subclasses broadly increased ≥ 2 -fold in corneal buttons within 24–48 h after scratching the corneal epithelium (mock infection) or HSV-1 infection (Fig. 6A). Increases were statistically significant in HSV-1-infected corneas at 48 h PI for IgA, IgG2a, and IgG3 (Fig. 6A). Notably, Ig concentrations in the avascular cornea prior to trauma or infection were an order of magnitude lower than the levels observed in healthy vascularized tissues, including the TG and ear pinna, after exsanguination (Supplemental Fig. 1). Moreover, elevations in total Ab concentration in the TG following HSV-1 infection (Supplemental Fig. 1A) or the ear following a hole-punch injury (Supplemental Fig. 1B) were subdued relative to the fluctuations observed in the cornea.

Sharp increases in total Ig within the cornea are consistent with our previous observations of transient edema following ocular

HSV-1 infection by ultrasound pachymetry (17, 31). In this study, we show that edema is prevalent within the corneal stroma at 24 h PI using in vivo SD-OCT imaging (Fig. 6B). Mast cells are associated with the pericorneal vasculature (Fig. 6C) and contribute to activation of the vascular endothelium through degranulation of potent vasoactive mediators, such as histamine and TNF- α , resulting in increased Ab perfusion (31, 41). Therefore, we evaluated the pericorneal mast cell activation status, as evidenced by degranulation in naive CD-1 mice, via confocal microscopy. Few degranulated mast cells were observed in healthy corneas, and intermittent degranulation was noted in mock-infected corneas; however, mast cell degranulation was widespread in HSV-1-infected corneas by 48 h PI (Fig. 6D), as previously reported in C57BL/6 mice (31). We interpret these observations to suggest that the increased perfusion of Ab in the cornea following infection is an active physiological response to ocular surface injury or infection.

Although Ab has been identified as a correlate of protection against HSV-1, the mechanism of the Ab effector function contributing to virus neutralization and clearance is not established for ocular infection. To further dissect this mechanism, we evaluated the relative contributions of complement fixation and Ab-dependent cell cytotoxicity (ADCC) with respect to viral clearance in vaccinated animals. Confocal microscopy was used to visualize complement activation in the corneas of CD-1 mice by colocalization of viral Ag and C3d, the final cleavage product of the complement cascade. C3d deposition is an established indicator of complement activation associated with Ab-mediated pathogen neutralization or opsonization (42, 43). Fewer viral lesions were observed in corneas from vaccinated animals compared with naive at 48 h PI (data not shown). Moreover, viral lesions were smaller in the corneas of HSV-1 0ΔNLS-vaccinated mice compared with immunologically naive mice following ocular HSV-1 challenge (Fig. 7A, 7B). Although the immunofluorescence signal of viral Ag was also diminished in vaccinated animals, this likely reflects epitope masking by endogenous HSV-specific Abs (Fig. 7A). Although strong C3d labeling was evident in corneas from vaccinated mice, labeling was absent in healthy corneas and sparse in corneas from naive mice at 48 h PI (Fig. 7A, 7B). Extensive colocalization between viral Ag and C3d was observed exclusively in corneas from animals vaccinated with HSV-1 0ΔNLS (Fig. 7B). Contrary to our expectations of finding typical surface-bound deposits of C3d, the C3d signal clustered within intracellular foci of corneal epithelial cells (Fig. 7A, 7B, Supplemental Video 1).

In addition to complement-fixation analysis, flow cytometry was used to assess cornea-infiltrating and tissue-resident leukocyte populations because of their potential to mediate ADCC. Limited differences were observed in leukocyte populations in the corneas of naive and immunized mice at 48 h PI (Fig. 7C). Fewer CD11b⁺ myeloid cells and, specifically, inflammatory monocytes were detected in corneas from HSV-1 0ΔNLS-immunized mice, although no differences were observed in the total number of macrophages, Langerhans cells, dendritic cells, or NK cells (Fig. 7C).

Given the apparent complement activation and presence of ADCC effector cells in the corneas of CD-1 mice vaccinated with HSV-1 0ΔNLS, we used C57BL/6 mice to further dissect the mechanism of protection. For these studies, WT, C3^{-/-}, and Fc γ RIII^{-/-} mice were vaccinated with HSV-1 0ΔNLS using a prime-boost immunization scheme in the footpad and flank, respectively, and subsequently challenged with 1×10^4 PFU HSV-1 strain McKrae per eye at day 30 postboost. Serum-neutralization titers were equivalent between sex-matched WT and C3^{-/-} or

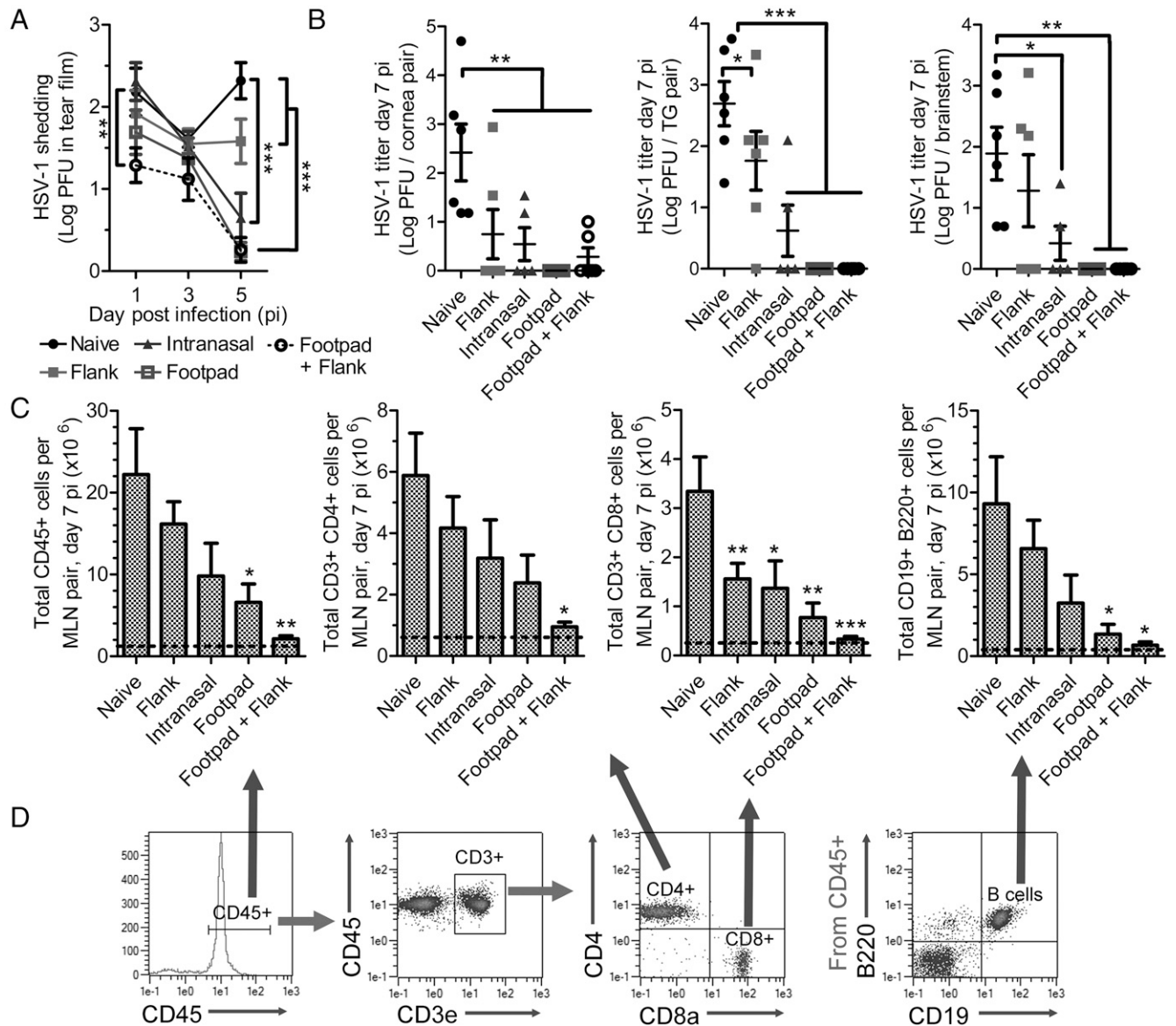


FIGURE 4. Immunization route impacts the protective efficacy of HSV-1 0 Δ NLS. Animals vaccinated in various tissues, as described in Fig. 3, were challenged with 1000 PFU HSV-1 McKrae per eye to evaluate viral shedding in the ocular tear film during the first 5 d PI (**A**) and were euthanized at day 7 PI to measure HSV-1 titers in the cornea, TG, and brainstem (**B**). Additionally, the cornea-draining MLNs were collected and processed by flow cytometry to assess lymphocyte proliferation (**C**); representative plots are shown in (**D**). Dashed lines reflect the mean value observed in MLNs from uninfected mice. Data are mean \pm SEM. Data in (**A**) represent $n = 6$ –16 per group, four independent experiments; data in (**B**) and (**C**) represent $n = 5$ or 6 mice per group, three independent experiments. * $p < 0.05$, ** $p < 0.01$, *** $p < 0.001$ versus the mean value of the naive control group, unless indicated otherwise, two-way ANOVA with the Bonferroni multiple-comparison test (**A**); one-way ANOVA with the Student–Newman–Keuls multiple-comparison test (**B** and **C**).

Fc γ RIII^{-/-} mice prior to ocular challenge (data not shown). Viral shedding in the tear film was assessed following HSV-1 challenge. A substantial delay in viral clearance was observed in vaccinated C3^{-/-} mice relative to WT (Fig. 7D). Viral clearance was equivalent between vaccinated WT and Fc γ RIII^{-/-} mice (Fig. 7E), thus downplaying the importance of classical Fc γ RIII (CD16)-dependent ADCC effector cells in prophylactic protection against HSV-1 in the cornea. Likewise, shedding was equivalent between immunologically naive WT and knockout mice, albeit at higher titers than observed in their respective vaccinated counterparts (Fig. 7D, 7E). Although the contributions of vaccine-induced humoral immunity in host defense against HSV-1 in the ocular mucosae are undoubtedly multifactorial, our data support a prominent role for the complement pathway in efficient prophylactic protection against HSV-1.

FcRn augments vaccine efficacy through IgG transport in the corneal epithelium

The barrier integrity of the cornea is maintained, in part, through tight junctional complexes between epithelial cells (39, 44). Although the intrinsic barrier property of the corneal epithelium protects the eye from the external environment, it concomitantly impedes macromolecule diffusion. Thus, the ability of Ab to passively diffuse into the corneal epithelium is restricted. Given the importance of maintaining the barrier integrity of the ocular surface, we explored the hypothesis that FcRn mediates Ab transcytosis within the corneal epithelium to facilitate humoral protection against HSV-1. Although FcRn is reportedly expressed at low levels in the cornea, its function remains enigmatic (45, 46).

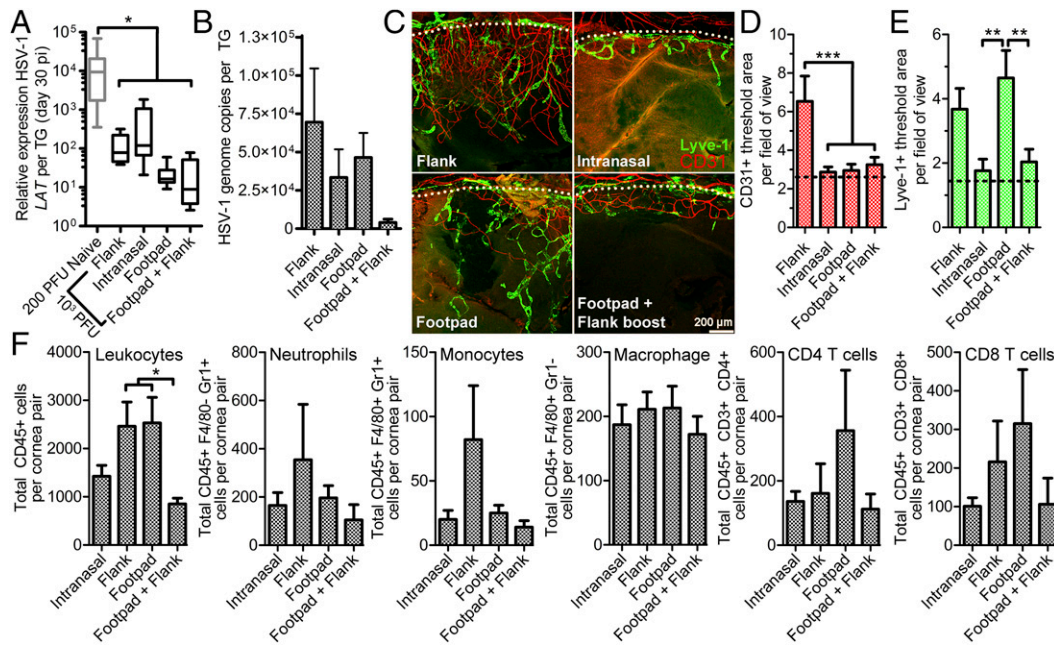


FIGURE 5. Routes of immunization govern the degree of protection against viral latency and tissue pathology upon ocular challenge. Animals were vaccinated in various tissues, as described in Fig. 3, and challenged with 1000 PFU HSV-1 McKrae per eye to evaluate the impact of immunization route on viral latency by LAT expression (**A**) or viral genome copy number (**B**) in the TG at day 30 PI. Corneas were imaged to evaluate neovascularization (**C**) and to quantify areas of hemangiogenesis (**D**) and lymphangiogenesis (**E**). Leukocyte populations in the cornea were also assessed by flow cytometry at day 30 PI (**F**). Data reflect mean \pm SEM, with the exception of the standard quartile-based box plot in (**A**); $n = 7$ or 8 TG per group with two independent experiments. Note that the values for naive animals in (**A**) reflect mice infected with only 200 PFU per eye. In (**B**), $n = 8$ –15 TG per group with two or three independent experiments; in (**C**)–(**E**), $n = 24$ –32 images from quadrants of six to eight flat-mounted corneas per group spanning two or three independent experiments; in (**F**), $n = 7$ –10 mice per group with three independent experiments. * $p < 0.05$, ** $p < 0.01$, *** $p < 0.001$, one-way ANOVA with the Student–Newman–Keuls multiple-comparisons test.

The expression profile of FcRn was first evaluated by confocal microscopy in cornea whole mounts from naive CD-1 mice before and after infection. FcRn expression was detected in the epithelium of healthy corneas, although expression was more conspicuous following HSV-1 infection (Fig. 8A). Intracellular FcRn expression was confirmed based on localization relative to actin filaments and nuclei in the corneal epithelium (Fig. 8A). Low-magnification imaging revealed that FcRn expression in the epithelium of healthy corneas decreased in a centripetal fashion from the periphery toward the center (Fig. 8B, top panels). In contrast, robust FcRn immunoreactivity was noted across the entire corneal epithelium in scratch-control and HSV-1-infected corneas at 24 h PI (Fig. 8B). Similar patterns of FcRn expression were observed in the corneal stroma (Fig. 8C). Strong colocalization of FcRn and HSV-1 Ag was observed within viral lesions on corneas from naive animals (Fig. 8D), suggesting that HSV-1 does not inhibit murine FcRn expression within infected cells. The specificity of the FcRn Ab for the p51 subunit was confirmed by Western blot (Fig. 8E) on lysates from uninfected and HSV-1-infected corneas (47).

FcRn expression profiles were subsequently evaluated quantitatively by flow cytometry in epithelial cells, Langerhans cells, and other leukocytes in cornea digests at 48 h PI (Fig. 8F). Basal FcRn expression was detected in CD45[−] epithelial cell adhesion molecule (EpcAM)⁺ corneal epithelial cells in uninfected mice based on median fluorescence intensity (MFI) relative to FMO background control levels (Fig. 8F, 8G). Consistent with the confocal data, FcRn expression levels increased by 30% in epithelial cells following ocular surface injury (mock infection scratch control) or HSV-1 infection (Fig. 8G). In addition, the total number of epithelial cells expressing FcRn increased nearly 2-fold following HSV-1 infection (Fig. 8G). Increases in basal FcRn expression

were also noted in the CD45⁺ EpcAM⁺ Langerhans cell population following corneal surface injury or infection (Fig. 8H). The observed FcRn MFI was comparatively negligible in the CD45⁺ EpcAM[−] population composed of resident and infiltrating leukocytes (Fig. 8I). This finding contrasts with the observation that myeloid lineage leukocytes in circulation express FcRn (48). To address these divergent findings, we evaluated FcRn expression with the same instrument settings in peripheral blood (Fig. 8J, 8K). Indeed, CD11b⁺ myeloid cells in circulation expressed much higher levels of FcRn (Fig. 8J) than were observed in the corneal CD45⁺ EpcAM[−] leukocyte population (Fig. 8I). PBLs were evaluated in parallel and found to express insignificant levels of FcRn (Fig. 8K). Peripheral blood CD11b⁺ myeloid cells were further profiled using Ly6C and Ly6G Ags to specifically confirm FcRn expression in circulating monocytes and neutrophils (Supplemental Fig. 2), the major populations of cornea-infiltrating cells during acute HSV-1 infection (49). Collectively, the confirmed upregulation of FcRn in the corneal epithelium provides a plausible mechanism to explain the protective capacity of Ab against HSV-1 in the cornea.

The protective contributions of FcRn were investigated by using siRNA to specifically target FcRn in the cornea. First, the knockdown efficiency of the topical FcRn siRNA treatment was confirmed in the corneas of naive CD-1 mice at 48 h PI relative to scramble control-treated animals by Western blot (Fig. 9A). Densitometry analysis indicated that FcRn protein levels were reduced in corneas treated with siRNA targeting FcRn compared with scramble control siRNA-treated mice (Fig. 9B). Local siRNA-mediated FcRn knockdown did not have an appreciable impact on total Ig concentrations within the corneas of naive mice following HSV-1 infection (Fig. 9C). However, FcRn knockdown in the corneas of mice vaccinated with HSV-1 Δ NLS severely

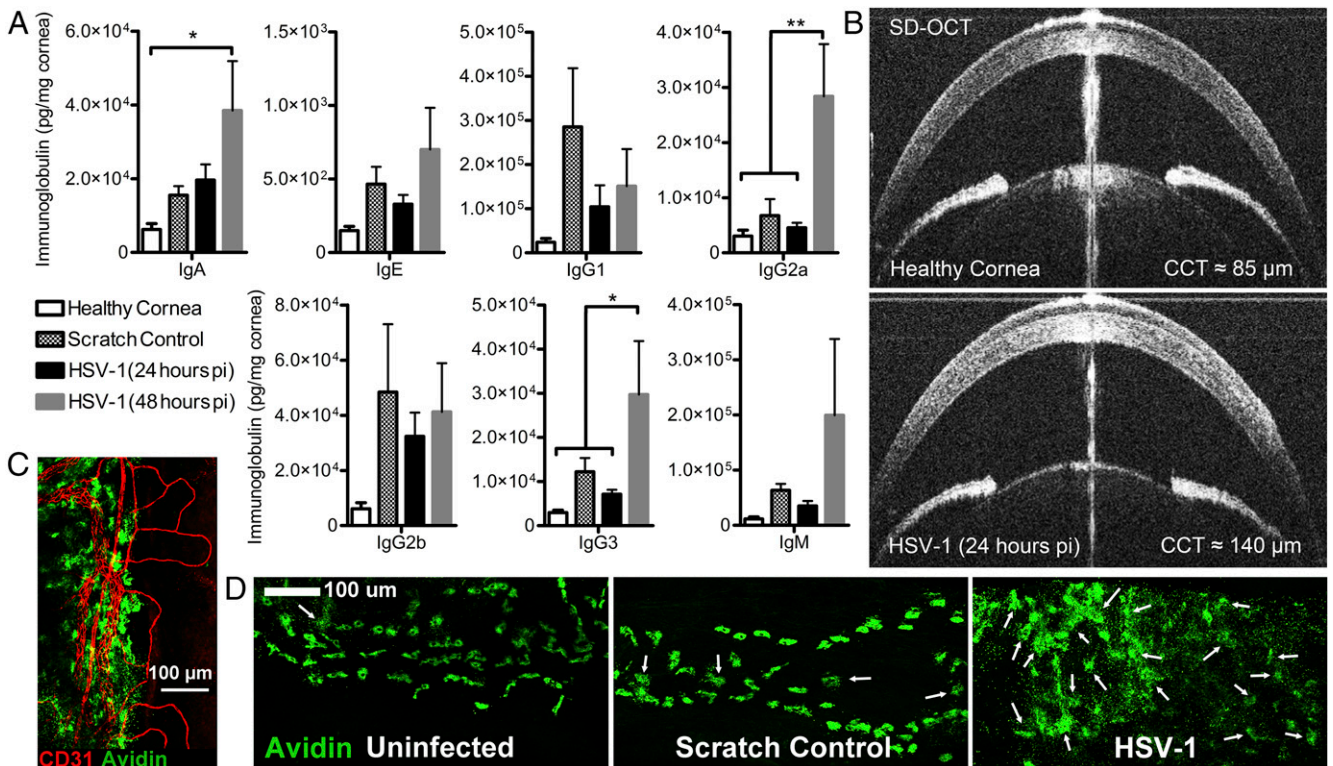


FIGURE 6. Ab-diffusion dynamics in the cornea following injury or infection. **(A)** Concentration of Ab by isotype in corneas from immunologically naive CD-1 mice reflecting healthy, scratch-control (24 h), and HSV-1-infected corneas ($n = 6$ or 7 cornea pairs per group; two or three independent experiments). **(B)** Representative photographs from SD-OCT imaging of the anterior segment of healthy and HSV-1-infected eyes showing corneal edema and prominent hyperintensities (leukocytic infiltrates) at 24 h PI. The central vertical line artifact is a Purkinje reflection, indicative of alignment with the corneal apex, which was used to control for consistency between eyes during image acquisition. **(C)** Avidin-labeled mast cells (green) reside along the cornea–sclera junction in close association with the CD31⁺ limbal blood vessels (red). **(D)** Confocal images of pericorneal mast cells in healthy, scratch-control, and HSV-1-infected corneas at 48 h PI. Arrows denote degranulated mast cells to highlight the widespread degranulation observed following HSV-1 infection. * $p < 0.05$, ** $p < 0.01$, one-way ANOVA with the Student–Newman–Keuls multiple-comparison test.

compromised the protective efficacy of the vaccine compared with the scramble control group (Fig. 9D). Explicitly, virus was detected in corneal homogenates by plaque assay in 100% of the FcRn siRNA-treated mice and only 25% of the scramble siRNA-treated mice (Fig. 9D). Nevertheless, the level of protection afforded to mice vaccinated with HSV-1 0ΔNLS after FcRn knockdown remained comparatively better than naive mice receiving either siRNA treatment, in terms of viral titer in the cornea at 48 h PI (Fig. 9D). Taken together, our data reveal a novel mechanism of vaccine-mediated protection against viral infection at the ocular surface involving FcRn. Although FcRn does not appear to be directly responsible for the observed influx of IgG into the cornea as a whole, its established role in Ab transcytosis is now appreciated to be a major factor in humoral immunity against infection within the mucosal epithelium of the ocular surface.

Discussion

Vaccine composition strongly influences the longevity of protection elicited by immunization, and this is likely dependent upon how a given vaccine “imprints” the immune system during the initial encounter to support plasma cell generation or memory B cell development (50). Epidemiological studies evaluating the kinetics of humoral responses to common vaccines in humans indicate that live-attenuated vaccines often offer life-long humoral protection against infection, whereas humoral responses elicited by subunit vaccines generally decay over time (34). Our recent work highlights that HSV-1 0ΔNLS was much more efficacious than a glycoprotein D-2 subunit vaccine, similar to that used in

multiple clinical trials, in limiting viral pathogenesis and preventing HSV-1-associated ocular disease in vaccinated mice challenged with HSV-1 (17); however, the kinetics of the humoral immune response was not evaluated in our previous study. In this article, we show that Ab titers elicited by a glycoprotein D-2 subunit vaccine decay substantially within 3 mo in mice, but HSV-1 0ΔNLS elicits sustained high titers of HSV-specific–neutralizing Ab. Interestingly, data from multiple clinical trials with glycoprotein D-2 subunit vaccines show that the cumulative mean HSV-specific and neutralizing Ab concentrations decay by ~85 and 77%, respectively, from peak titers within 1 y of the last dose (51). Furthermore, even with a live-attenuated virus, the site of vaccination has an important effect on the induction of humoral immunity and efficacy (Figs. 3–5). Despite i.m. injection being the most common route of vaccination clinically, HSV-1 0ΔNLS was least effective following i.m. vaccination alone. In contrast, near-complete protection against acute disease and viral latency was achieved with HSV-1 0ΔNLS following s.c. primary immunization with an i.m. boost; however, vaccine efficacy and safety must be weighed in light of the status of the recipient’s immune system. Subunit vaccines may be preferred over attenuated vaccines for immunocompromised patients because of safety concerns. Additionally, immunosenescence is documented to limit the efficacy of ZOSTAVAX, a therapeutic live-attenuated shingles vaccine, relative to a novel subunit vaccine in older adults (52).

In addition to their limited antigenic breadth, the ephemeral nature of humoral responses elicited by past HSV subunit vaccines is a likely reason for the widespread failure of such vaccines in multiple clinical trials (8, 53). Subunit vaccines, such as the alum-

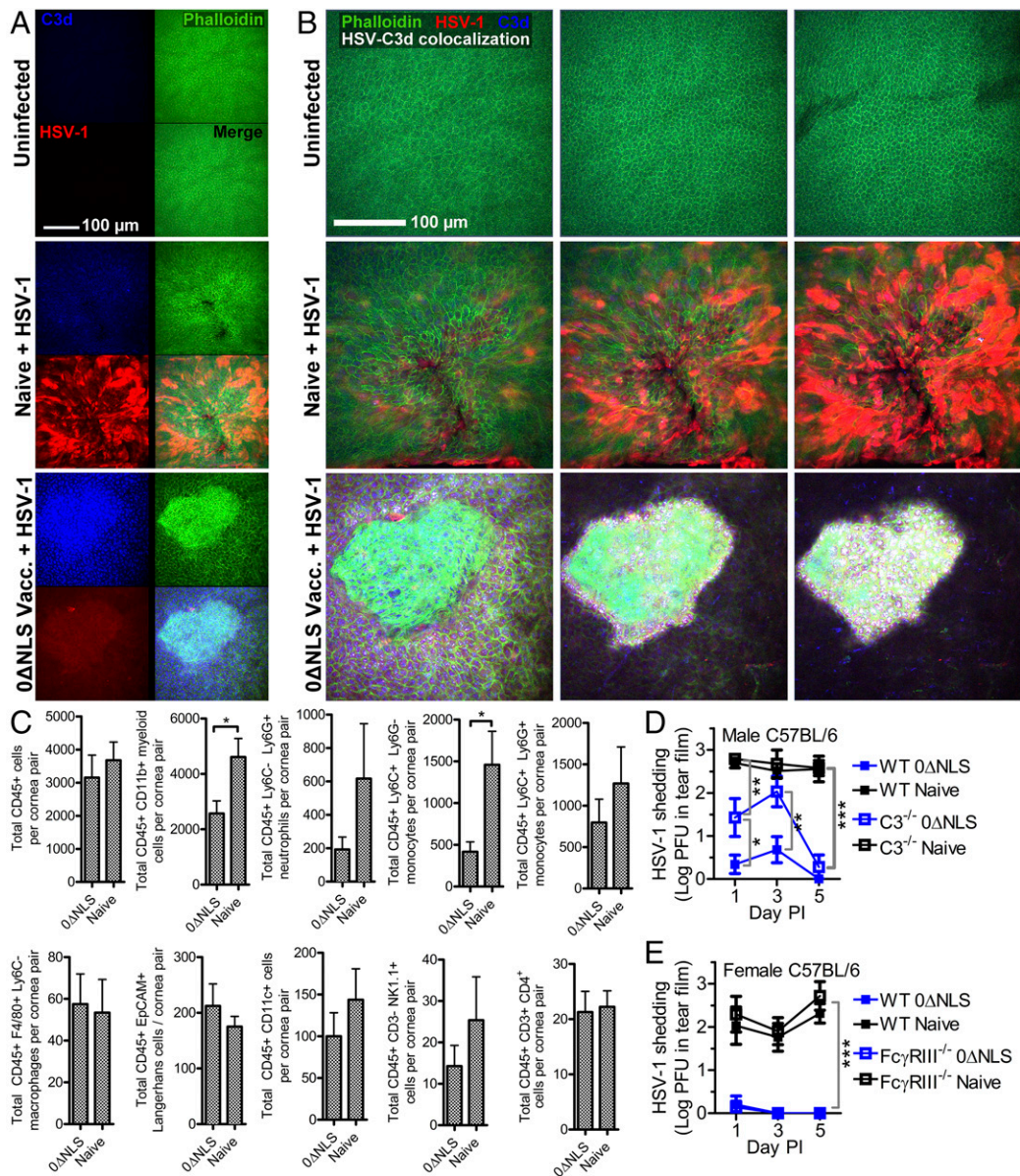


FIGURE 7. Complement mediates humoral protection against ocular HSV-1 infection. **(A)** Representative confocal images centered above apparent viral lesions showing C3d (blue) and HSV-1 Ag (red) in healthy or HSV-1-infected corneas at 48 h PI with phalloidin (green) staining to delineate cell boundaries. Naive reflects HSV-infected immunologically naive mice. 0ΔNLS Vacc. reflects mice that were immunized in the footpad, boosted in the flank with HSV-1 0ΔNLS, and infected 30 d later with 1000 PFU HSV-1 McKrae in the eye. **(B)** Individual z-slices of representative composite image shown in (A), with colocalization of HSV-1 and C3d, calculated using Imaparis, displayed as white overlay. Images are representative of four to six corneas per group. **(C)** Flow cytometry was used to characterize various leukocyte populations in the corneas of immunologically naive and HSV-1 0ΔNLS-vaccinated mice immunized at 48 h PI. Populations represented include total CD45⁺ leukocytes, CD11b⁺ myeloid cells, Ly6G⁺ neutrophils, Ly6C⁺ monocytes, F4/80⁺ macrophages, CD45⁺ EPCAM⁺ Langerhans cells, CD11c⁺ dendritic cells, CD3⁻ NK1.1⁺ NK cells, and CD4⁺ T cells. Data are mean ± SEM for seven or eight mice per group; three independent experiments. **p* < 0.05, Student *t* test. Data in (A)–(C) reflect CD-1 mice. Given the evidence for complement activation and the presence of ADCC effector cells in the corneas of vaccinated CD-1 mice, C57BL/6 mice were subsequently used to assess viral clearance/shedding and the effector mechanism of humoral protection in the tear film of naive and HSV-1 0ΔNLS-vaccinated WT and C3^{-/-} mice **(D)** or WT and FcγRIII^{-/-} mice **(E)**. Data reflect five mice per group; two independent experiments. **p* < 0.05, ***p* < 0.01, ****p* < 0.001, two-way ANOVA with the Bonferroni multiple-comparisons test.

adjuvanted hepatitis B surface Ag vaccine, can be highly effective against disease, despite waning or undetectable Ab titers through anamnestic responses. A meta-analysis of subjects vaccinated with hepatitis B surface Ag clearly links anamnestic responses to protection against disease in patients who seroconvert for other hepatitis B Ags (54). The partial, yet incomplete, protective effect elicited by a glycoprotein D-2 subunit vaccine presumably functions through an anamnestic response; however, anamnestic responses are likely too little too late in the case of HSV-1 infection,

because the virus can quickly transfer from mucosal epithelial cells to nerve ganglia, where the virus persists indefinitely. Moreover, anamnestic responses against the glycoprotein D-2 subunit reflect ~1% of the HSV-1 proteome, whereas the antigenic coverage of the hepatitis B surface Ag is 12% (53). In contrast, the HSV-1 0ΔNLS vaccine encodes nearly 99% of the native viral proteome and elicits humoral immune responses similar to those observed during natural infection (17, 18). Results in this article from a delayed challenge model mirror previous data showing that the HSV-1 0ΔNLS vac-

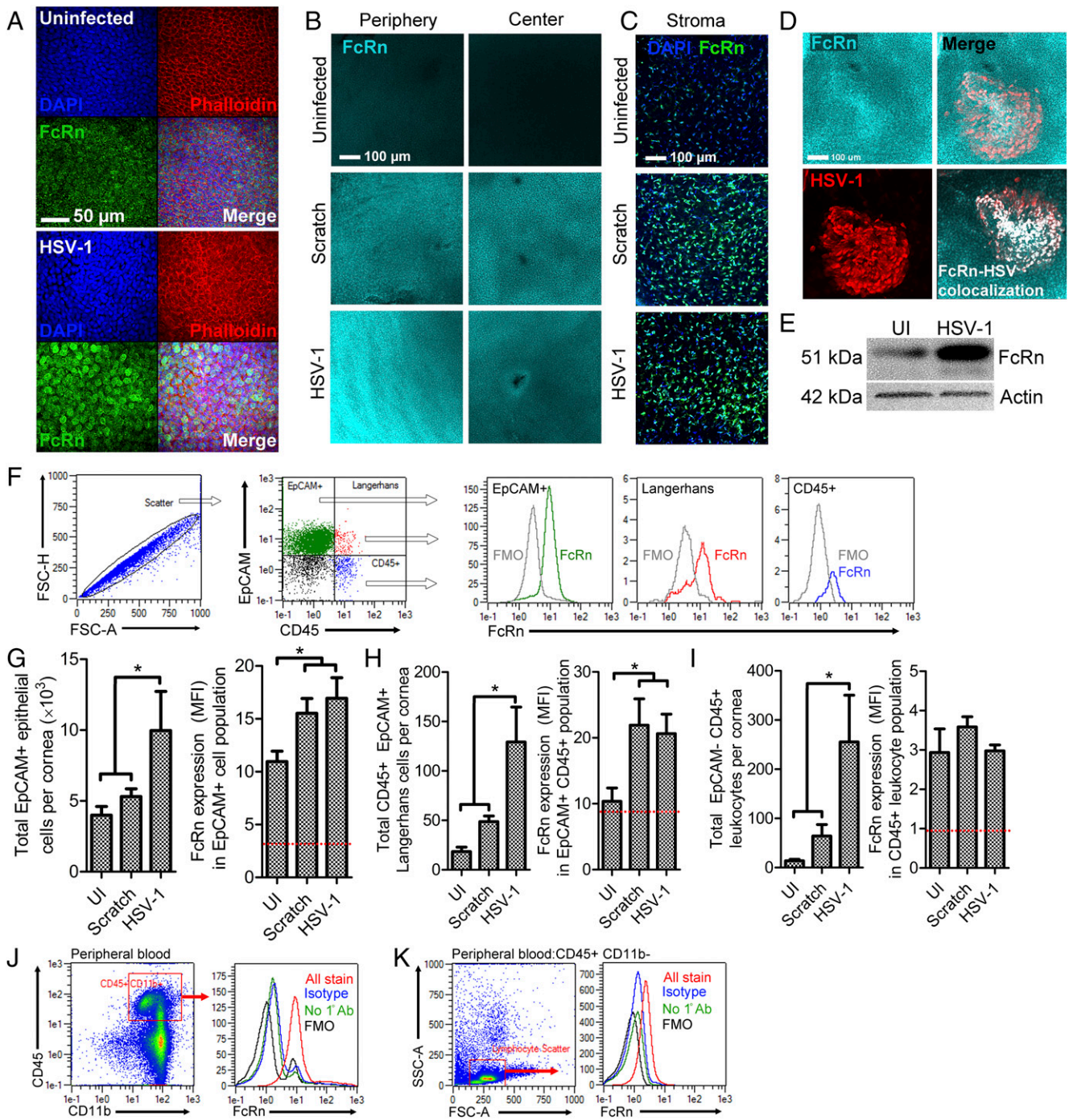


FIGURE 8. FcRn is upregulated in the cornea following injury or infection. **(A)** Representative confocal images of FcRn (green) labeling in the epithelium of healthy uninfected and HSV-1-infected corneas at 48 h PI. DAPI (blue) and phalloidin (red) staining was used to identify tissue boundaries and borders. **(B)** Representative low-magnification confocal images showing the radial patterning of FcRn expression (cyan) in the healthy corneal epithelium (peripheral expression > central) and its widespread elevated expression in mock-infected (scratch control) or HSV-1-infected corneas. **(C)** FcRn expression (cyan) in the deeper stromal keratocyte layer is also upregulated following corneal injury or infection. **(D)** Colocalization of FcRn (cyan) and HSV-1 Ag (red) was observed within the corneal epithelium of naive CD-1 mice and digitally confirmed using Imapar software to verify pixel overlap (white overlay, lower right panel). Images shown in **(B)–(D)** are representative of four to six labeled corneas per group. **(E)** Western blot confirmation of FcRn Ab specificity showing the p51 subunit of FcRn in digests from healthy and HSV-1-infected corneal digests (48 h PI). Actin labeling was used as a loading control, with 20 μ g of total protein input per sample. **(F)** Gating strategy for FcRn analysis by flow cytometry, including scatter profile for doublet discrimination, selection of cell subsets (EpCAM⁺ CD45⁻ epithelial cells, EpCAM⁺ CD45⁺ Langerhans cells, or EpCAM⁻ CD45⁺ leukocytes), and downstream quantification of FcRn MFI relative to FMO background controls. Summary of flow cytometry data quantifying the total number of cells and MFI of FcRn expression for epithelial cells **(G)**, Langerhans cells **(H)**, and other leukocytes **(I)** in corneal digests; ($n = 5$ or 6 corneas per group; three independent experiments). Data in **(G)–(I)** reflect mean \pm SEM. Flow cytometry was used to assess FcRn expression in peripheral blood CD45⁺ CD11b⁺ myeloid cells **(J)** and CD45⁺ lymphocytes based on scatter profile **(K)**; data are representative of three independent experiments. * $p < 0.05$, one-way ANOVA with the Student–Newman–Keuls multiple-comparisons test.

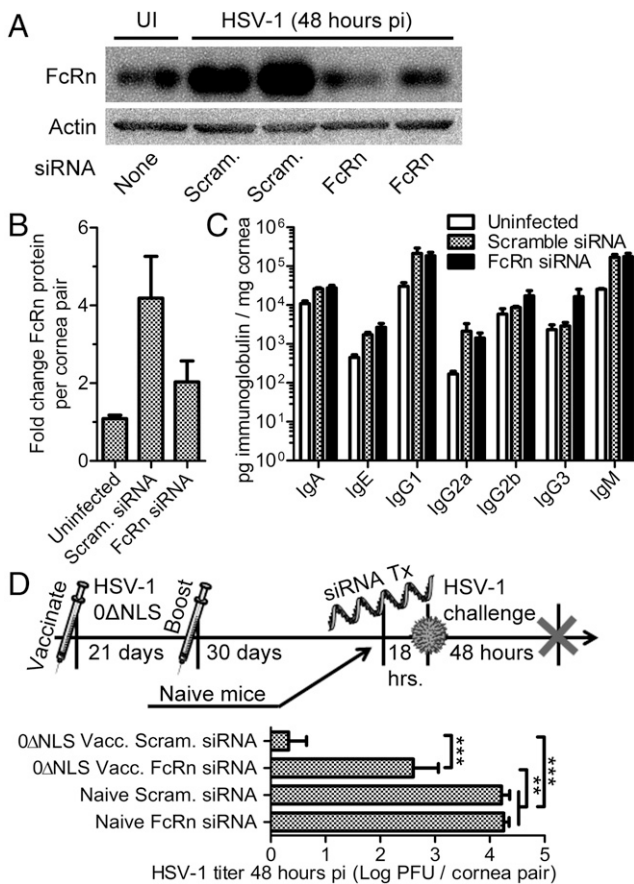


FIGURE 9. FcRn is essential for humoral protection against HSV-1 in the cornea. **(A)** Corneas of naive CD-1 mice were treated topically with nonspecific scramble control siRNA (Scram.) or FcRn-specific siRNA and infected with HSV-1; tissue was assessed at 48 h PI for FcRn protein content by Western blot to confirm knockdown efficiency. **(B)** Quantitative summary of FcRn-knockdown efficiency using densitometric analysis of FcRn blots relative to actin loading controls and normalized to healthy uninfected corneas; $n = 4$ naive mice per group, $n = 7$ scrambled siRNA-treated mice per group, and $n = 8$ FcRn siRNA-treated mice per group (three independent experiments). **(C)** Tissue lysates from **(A)** were evaluated for total Ig content, as described in Fig. 6, to determine the contributions of FcRn to Ab perfusion into the cornea. **(D)** Timeline depicts siRNA treatment in naive and vaccinated (HSV-1 0ΔNLS footpad-flank prime-boost regimen) CD-1 mice, ocular HSV-1 challenge (1000 PFU HSV-1 McKrae), and tissue collection at 48 h PI. Corneas were assessed for viral burden by plaque assay; $n = 4$ or 5 mice per group (two independent experiments). **(D)** was prepared using Servier Medical Art (www.servier.com) via Creative Commons 3.0. $^{**}p < 0.01$, $^{***}p < 0.001$, one-way ANOVA with the Student–Newman–Keuls multiple-comparisons test. UI, uninfected cornea.

cine can prevent corneal sensation loss and neovascularization; however, our data show that the immune response elicited by HSV-1 0ΔNLS sustains its protective effect over time (Fig. 1C).

Although IgG is found throughout the cornea, the distribution of IgM and IgA is restricted to the corneal periphery and apical surface epithelium, respectively (21, 55). Concentrations of IgG in the central region of healthy corneas are approximately two thirds of those found in the periphery, but the basal diffusion rate of IgG in the cornea is low (40, 56, 57). This is evidenced by the limited clinical success of IgG-based therapeutics in the cornea. Although the general mechanisms of ocular surface protection have been reviewed elsewhere (58–60), secretory IgA is commonly associated with humoral protection against microbial infection in the tear film and in other mucosal sites (61, 62). Clinical and basic

research data confirm that serum titers of HSV-specific IgA do not correlate with susceptibility to primary HSV infection after vaccination or viral reactivation in latently infected hosts (63–65).

Protein diffusion in the cornea has largely been calculated experimentally using IgG and albumin (56, 57, 66, 67); however, FcRn is responsible for the bidirectional transport of both proteins (68, 69). Coupling the results from the current study identifying FcRn expression changes during viral infection or surface injury, we postulate that FcRn expression levels largely regulate IgG (and albumin) diffusion in the corneal epithelium. This insight into the kinetics of IgG perfusion in the cornea may enhance the usefulness of Ab-based therapies that normally have low corneal penetration and efficacy if combined with adjuvant therapy to modulate FcRn expression in the surface epithelium barrier. Furthermore, this approach could enhance the “depot effect” of IgG-based therapeutics in the cornea described by Osusky et al. (57) to increase drug half-life and local efficacy.

The pericorneal limbal vasculature is well documented as the source of Ab within the cornea, given the comparatively low concentrations of IgG in the adjacent tear film and aqueous humor (40, 70). It is estimated that it takes 50–70 d for serum IgG to establish a concentration equilibrium with IgG in the cornea under normal homeostatic conditions (40, 57). Given this low basal rate of diffusion, it is clear that a prophylactic HSV-1 vaccine must elicit and sustain high serum concentrations of protective IgG to provide a tenable level of protection in the cornea. However, this limitation may be partially overcome by physiological mechanisms that enhance IgG diffusion in the cornea during infection, particularly upregulation of FcRn in the epithelium. In this article, we demonstrate that the Ab concentration in the cornea rises sharply following corneal infection or injury and that this phenomenon is concomitant with FcRn upregulation in various cornea-resident cell populations (Figs. 6 and 8). Indeed, local FcRn knockdown compromises the efficacy of humoral protection elicited by HSV-1 0ΔNLS (Fig. 9). Previous studies showed that FcRn facilitates intracellular neutralization of viruses within mucosal epithelial cells in passively immunized animals (71). FcRn expression has also been correlated with passive humoral protection against HSV-2 infection in the vaginal mucosae (72). However, there are caveats to using global FcRn-deficient mice for passive-immunization studies, because Ab half-life is severely impacted (23). Accordingly, our studies used localized FcRn knockdown to determine the effect of FcRn on viral clearance (Fig. 9). It remains unclear why cornea-infiltrating leukocytes express much lower levels of FcRn than are observed in circulating leukocytes (Fig. 8I, 8J); it is tempting to speculate that leukocytes store Ab in circulation via FcRn-mediated retention for discharge upon activation and extravasation into inflamed tissues, as they are proposed to do with soluble complement components (73).

Consistent with the role of FcRn in intracellular trafficking of IgG, we also observed intracellular deposition of C3d in the corneal epithelium of HSV-1 0ΔNLS-vaccinated mice following ocular challenge (Fig. 7A, 7B, Supplemental Video 1). Although complement deposition classically occurs on the cell surface, evidence is mounting that intracellular complement signaling (dubbed the “complosome”) serves multiple functions (74–77). Our data also show that prophylactic protection against HSV-1 is compromised in the absence of a functional complement pathway in the cornea (Fig. 7D). Although the complement pathway reportedly enhances humoral immunity during primary HSV-1 infection, the role of complement in prophylactic protection against HSV-1 infection in the eye has not been previously reported (78–81). The ability of complement to enhance neutralization of HSV-1 virions is thought to be limited by the viral glycoproteins that mimic the IgG Fc receptor and

interact with C3 to modulate complement activation (81, 82). Despite these viral immune-evasion mechanisms, Ab retains its capacity to neutralize HSV-1 in patients vaccinated with a glycoprotein D-2 subunit vaccine (27); however, the role of complement may be dependent upon the site of virus entry, because other investigators have demonstrated that ADCC is central to protection against HSV-1, using a skin infection model (83).

Recent findings demonstrate that intracellular Ab-bound viral components are shuttled to the proteasome by the intracellular effector tripartite motif-containing 21 for noncytolytic viral clearance (84). FcRn recycling may enable sufficient internalization of Ab within mucosal epithelial cells to facilitate targeting and degradation of diverse viral proteins. This concept challenges the dogma that Ab mediates protective effects exclusively in the extracellular space. Additionally, the concept of Ab actively targeting viral proteins intracellularly also begs the question of whether intracellular epitopes should be targeted in vaccine development against other mucosal pathogens to enhance humoral protection. These questions will need to be addressed in future studies.

Although Ab mediates prophylactic protection against primary ocular HSV-1 infection, it remains unknown why Ab responses fail to protect patients who experience frequent HSV-1 reactivation in the eye. Uncovering the central role of FcRn in Ab-mediated protection against HSV-1 may provide insight into this conundrum. Ocular immunopathology associated with recurrent corneal HSV-1 reactivation in humans is driven primarily by TLR signaling and CD4 T cells (9). In vitro studies have demonstrated that FcRn expression is upregulated by TNF- α and repressed by IFN- γ in polarized epithelial cells (85, 86). Therefore, the establishment of tissue-resident CD4 T cells in the corneas of patients with frequent HSV-1 reactivation may, in fact, limit the expression of FcRn via IFN- γ expression and consequently usurp the local protective functions of Ab. Although HSV-1 Δ NLS has strong translational potential, diverse vaccine strategies will undoubtedly emerge and continue to augment HSV-1 vaccine development. It is now evident that a successful prophylactic HSV-1 vaccine must be capable of eliciting a long-lived, high-titer humoral immune response to effectively combat ocular disease and limit neuroinvasion. Irrespective of whether the Ab-mediated effector function protects via complement, ADCC, intracellular targeting, or a combination thereof, Ab persistence following vaccination is a critical limiting factor of prophylactic vaccine efficacy against HSV-1 infection (87).

Acknowledgments

We thank the Dean McGee Eye Institute vivarium staff for maintaining our animal colonies, Edward Gershburg for supplying the recombinant glycoprotein D-2 protein, and the late Brian Gebhardt for contributing the original stock of HSV-1 McKrae.

Disclosures

W.P.H. is a cofounder of Rational Vaccines, Inc., which has licensed U.S. patents 77856605 and 8802109, and is a coauthor on U.S. patent 8802109, which describes the uses of HSV mutant ICP0 in the design of a live attenuated HSV-2 vaccine strain. D.J.J.C. is a member of the advisory board of Rational Vaccines, Inc. and will be provided stock options in the future. The other authors have no financial conflicts of interest.

References

- Iwasaki, A. 2016. Exploiting mucosal immunity for antiviral vaccines. *Annu. Rev. Immunol.* 34: 575–608.
- Su, F., G. B. Patel, S. Hu, and W. Chen. 2016. Induction of mucosal immunity through systemic immunization: phantom or reality? *Hum. Vaccin. Immunother.* 12: 1070–1079.
- Czerkinsky, C., and J. Holmgren. 2010. Topical immunization strategies. *Mucosal Immunol.* 3: 545–555.
- Neutra, M. R., and P. A. Kozlowski. 2006. Mucosal vaccines: the promise and the challenge. *Nat. Rev. Immunol.* 6: 148–158.
- Belyakov, I. M., and J. D. Ahlers. 2009. What role does the route of immunization play in the generation of protective immunity against mucosal pathogens? *J. Immunol.* 183: 6883–6892.
- Forrester, J. V., A. D. Dick, P. G. McMenamin, F. Roberts, and E. Pearlman. 2016. *The Eye: Basic Sciences in Practice*, 4th Ed. Elsevier, London.
- Whitcher, J. P., M. Srinivasan, and M. P. Upadhyay. 2001. Corneal blindness: a global perspective. *Bull. World Health Organ.* 79: 214–221.
- Royer, D. J., A. Cohen, and D. Carr. 2015. The current state of vaccine development for ocular HSV-1 infection. *Expert Rev. Ophthalmol.* 10: 113–126.
- Farooq, A. V., and D. Shukla. 2012. Herpes simplex epithelial and stromal keratitis: an epidemiologic update. *Surv. Ophthalmol.* 57: 448–462.
- Lairson, D. R., C. E. Begley, T. F. Reynolds, and K. R. Wilhelmus. 2003. Prevention of herpes simplex virus eye disease: a cost-effectiveness analysis. *Arch. Ophthalmol.* 121: 108–112.
- Caselli, E., P. G. Balboni, C. Incorvaia, R. Argani, F. Parmeggiani, E. Cassai, and R. Manservigi. 2000. Local and systemic inoculation of DNA or protein gB1s-based vaccines induce a protective immunity against rabbit ocular HSV-1 infection. *Vaccine* 19: 1225–1231.
- Keadle, T. L., K. A. Laycock, J. K. Miller, K. K. Hook, E. D. Fenoglio, M. Francotte, M. Slaoui, P. M. Stuart, and J. S. PePOSE. 1997. Efficacy of a recombinant glycoprotein D subunit vaccine on the development of primary and recurrent ocular infection with herpes simplex virus type 1 in mice. *J. Infect. Dis.* 176: 331–338.
- Chentoufi, A. A., G. Dasgupta, N. D. Christensen, J. Hu, Z. S. Choudhury, A. Azeem, J. V. Jester, A. B. Nesburn, S. L. Wechsler, and L. BenMohamed. 2010. A novel HLA (HLA-A*0201) transgenic rabbit model for preclinical evaluation of human CD8⁺ T cell epitope-based vaccines against ocular herpes. *J. Immunol.* 184: 2561–2571.
- Walker, J., and D. A. Leib. 1998. Protection from primary infection and establishment of latency by vaccination with a herpes simplex virus type 1 recombinant deficient in the virion host shutoff (vhs) function. *Vaccine* 16: 1–5.
- Nesburn, A. B., T. V. Ramos, X. Zhu, H. Asgarzadeh, V. Nguyen, and L. BenMohamed. 2005. Local and systemic B cell and Th1 responses induced following ocular mucosal delivery of multiple epitopes of herpes simplex virus type 1 glycoprotein D together with cytosine-phosphate-guanine adjuvant. *Vaccine* 23: 873–883.
- Bettahi, I., A. B. Nesburn, S. Yoon, X. Zhang, A. Mohebbi, V. Sue, A. Vanderberg, S. L. Wechsler, and L. BenMohamed. 2007. Protective immunity against ocular herpes infection and disease induced by highly immunogenic self-adjuvanting glycoprotein D lipopeptide vaccines. *Invest. Ophthalmol. Vis. Sci.* 48: 4643–4653.
- Royer, D. J., H. R. Gurung, J. K. Jenkins, J. J. Geltz, J. L. Wu, W. P. Halford, and D. J. Carr. 2016. A highly efficacious herpes simplex virus 1 vaccine blocks viral pathogenesis and prevents corneal immunopathology via humoral immunity. *J. Virol.* 90: 5514–5529.
- Royer, D. J., M. M. Carr, A. J. Chucair-Elliott, W. P. Halford, and D. J. Carr. 2017. Impact of type 1 interferon on the safety and immunogenicity of an experimental live-attenuated herpes simplex virus type 1 vaccine in mice. *J. Virol.* 91: e02342–e02416.
- Belshe, R. B., T. C. Heineman, D. I. Bernstein, A. R. Bellamy, M. Ewell, R. van der Most, and C. D. Deal. 2014. Correlate of immune protection against HSV-1 genital disease in vaccinated women. *J. Infect. Dis.* 209: 828–836.
- Plotkin, S. A., W. A. Orenstein, and P. A. Offit, eds. 2013. *Vaccines*, 6th Ed. Elsevier Saunders, Philadelphia.
- Allansmith, M. R., and B. H. McClellan. 1975. Immunoglobulins in the human cornea. *Am. J. Ophthalmol.* 80: 123–132.
- Preston, M. J., K. A. Kernacki, J. M. Berk, L. D. Hazlett, and R. S. Berk. 1992. Kinetics of serum, tear, and corneal antibody responses in resistant and susceptible mice intracorneally infected with *Pseudomonas aeruginosa*. *Infect. Immun.* 60: 885–891.
- Roopenian, D. C., and S. Akilesh. 2007. FcRn: the neonatal Fc receptor comes of age. *Nat. Rev. Immunol.* 7: 715–725.
- Aldinger, K. A., G. Sokoloff, D. M. Rosenberg, A. A. Palmer, and K. J. Millen. 2009. Genetic variation and population substructure in outbred CD-1 mice: implications for genome-wide association studies. *PLoS One* 4: e4729.
- Yao, H.-W., P. Ling, S.-H. Chen, Y.-Y. Tung, and S.-H. Chen. 2012. Factors affecting herpes simplex virus reactivation from the explanted mouse brain. *Virology* 433: 116–123.
- Halford, W. P., R. Püschel, E. Gershburg, A. Wilber, S. Gershburg, and B. Rakowski. 2011. A live-attenuated HSV-2 ICP0 virus elicits 10 to 100 times greater protection against genital herpes than a glycoprotein D subunit vaccine. *PLoS One* 6: e17748.
- Awasthi, S., R. B. Belshe, and H. M. Friedman. 2014. Better neutralization of herpes simplex virus type 1 (HSV-1) than HSV-2 by antibody from recipients of GlaxoSmithKline HSV-2 glycoprotein D2 subunit vaccine. *J. Infect. Dis.* 210: 571–575.
- Bryant-Hudson, K. M., and D. J. Carr. 2012. CXCL1-deficient mice are highly sensitive to *Pseudomonas aeruginosa* but not herpes simplex virus type 1 corneal infection. *Invest. Ophthalmol. Vis. Sci.* 53: 6785–6792.
- Downie, L. E., M. J. Stainer, and H. R. Chinnery. 2014. Monitoring of strain-dependent responsiveness to TLR activation in the mouse anterior segment using SD-OCT. *Invest. Ophthalmol. Vis. Sci.* 55: 8189–8199.
- Wuest, T. R., and D. J. Carr. 2010. VEGF-A expression by HSV-1-infected cells drives corneal lymphangiogenesis. *J. Exp. Med.* 207: 101–115.
- Royer, D. J., M. Zheng, C. D. Conrady, and D. J. Carr. 2015. Granulocytes in ocular HSV-1 infection: opposing roles of mast cells and neutrophils. *Invest. Ophthalmol. Vis. Sci.* 56: 3763–3775.

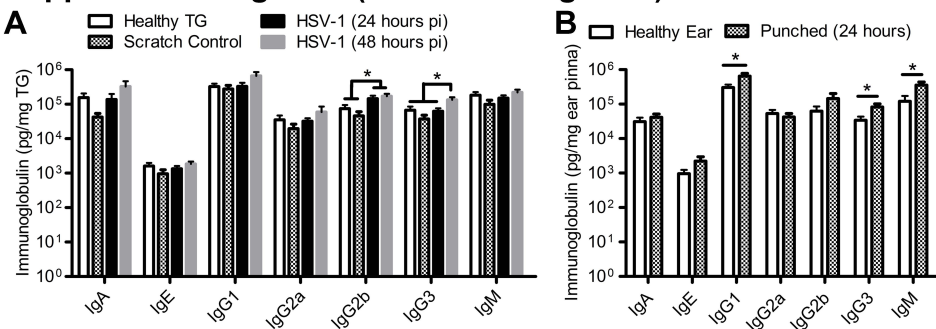
32. Royer, D. J., C. D. Conrady, and D. J. Carr. 2016. Herpesvirus-associated lymphadenitis distorts fibroblastic reticular cell microarchitecture and attenuates CD8 T cell responses to neurotropic infection in mice lacking the STING-IFN α / β defense pathways. *J. Immunol.* 197: 2338–2352.
33. Royer, D. J., and D. J. Carr. 2016. A STING-dependent innate-sensing pathway mediates resistance to corneal HSV-1 infection via upregulation of the antiviral effector tetherin. *Mucosal Immunol.* 9: 1065–1075.
34. Amanna, I. J., N. E. Carlson, and M. K. Slifka. 2007. Duration of humoral immunity to common viral and vaccine antigens. *N. Engl. J. Med.* 357: 1903–1915.
35. Hamrah, P., A. Cruzat, M. H. Dastjerdi, L. Zheng, B. M. Shahatit, H. A. Bayhan, R. Dana, and D. Pavan-Langston. 2010. Corneal sensation and subbasal nerve alterations in patients with herpes simplex keratitis: an in vivo confocal microscopy study. *Ophthalmology* 117: 1930–1936.
36. Chucair-Elliott, A. J., M. Zheng, and D. J. Carr. 2015. Degeneration and regeneration of corneal nerves in response to HSV-1 infection. *Invest. Ophthalmol. Vis. Sci.* 56: 1097–1107.
37. Goldstein, D. A., A. A. Mis, F. S. Oh, and J. G. Deschenes. 2009. Persistent pupillary dilation in herpes simplex uveitis. *Can. J. Ophthalmol.* 44: 314–316.
38. Thiel, M. A., D. J. Coster, S. D. Standfield, H. M. Brereton, C. Mavragelos, H. Zola, S. Taylor, A. Yusim, and K. A. Williams. 2002. Penetration of engineered antibody fragments into the eye. *Clin. Exp. Immunol.* 128: 67–74.
39. Gaudana, R., H. K. Ananthula, A. Parenky, and A. K. Mitra. 2010. Ocular drug delivery. *AAPS J.* 12: 348–360.
40. Verhagen, C., A. C. Breeboort, and A. Kijlstra. 1990. Diffusion of immunoglobulin G from the vascular compartment into the normal rabbit cornea. *Invest. Ophthalmol. Vis. Sci.* 31: 1519–1525.
41. Frossi, B., F. Mion, C. Tripodo, M. P. Colombo, and C. E. Pucillo. 2017. Rheostatic functions of mast cells in the control of innate and adaptive immune responses. *Trends Immunol.* DOI: 10.1016/j.it.2017.04.001.
42. Toapanta, F. R., and T. M. Ross. 2006. Complement-mediated activation of the adaptive immune responses: role of C3d in linking the innate and adaptive immunity. *Immunol. Res.* 36: 197–210.
43. Zhang, R., Z. Y. Zheng, J. S. Lin, L. J. Qu, and F. Zheng. 2012. The continual presence of C3d but not IgG glomerular capillary deposition in stage I idiopathic membranous nephropathy in patients receiving corticosteroid treatment. *Diagn. Pathol.* 7: 109.
44. Zihni, C., C. Mills, K. Matter, and M. S. Balda. 2016. Tight junctions: from simple barriers to multifunctional molecular gates. *Nat. Rev. Mol. Cell Biol.* 17: 564–580.
45. Kim, H., R. N. Fariss, C. Zhang, S. B. Robinson, M. Thill, and K. G. Csaky. 2008. Mapping of the neonatal Fc receptor in the rodent eye. *Invest. Ophthalmol. Vis. Sci.* 49: 2025–2029.
46. Pownier, M. B., J. A. McKenzie, G. J. Christianson, D. C. Roopenian, and M. Fruttiger. 2014. Expression of neonatal Fc receptor in the eye. *Invest. Ophthalmol. Vis. Sci.* 55: 1607–1615.
47. Simister, N. E., and K. E. Mostov. 1989. An Fc receptor structurally related to MHC class I antigens. *Nature* 337: 184–187.
48. Zhu, X., G. Meng, B. L. Dickinson, X. Li, E. Mizoguchi, L. Miao, Y. Wang, C. Robert, B. Wu, P. D. Smith, et al. 2001. MHC class I-related neonatal Fc receptor for IgG is functionally expressed in monocytes, intestinal macrophages, and dendritic cells. *J. Immunol.* 166: 3266–3276.
49. Conrady, C. D., M. Zheng, N. A. Mandal, N. van Rooijen, and D. J. Carr. 2013. IFN- α -driven CCL2 production recruits inflammatory monocytes to infection site in mice. *Mucosal Immunol.* 6: 45–55.
50. Amanna, I. J., and M. K. Slifka. 2010. Mechanisms that determine plasma cell lifespan and the duration of humoral immunity. *Immunol. Rev.* 236: 125–138.
51. Belshe, R. B., P. A. Leone, D. I. Bernstein, A. Wald, M. J. Levin, J. T. Stapleton, I. Gorfinkel, R. L. A. Morrow, M. G. Ewell, A. Stokes-Riner, et al; Herpesvacc Trial for Women. 2012. Efficacy results of a trial of a herpes simplex vaccine. *N. Engl. J. Med.* 366: 34–43.
52. Lal, H., A. L. Cunningham, O. Godeaux, R. Chlibek, J. Diez-Domingo, S.-J. Hwang, M. J. Levin, J. E. McElhaney, A. Poder, J. Puig-Barberà, et al; ZOE-50 Study Group. 2015. Efficacy of an adjuvanted herpes zoster subunit vaccine in older adults. *N. Engl. J. Med.* 372: 2087–2096.
53. Halford, W. P. 2014. Antigenic breadth: a missing ingredient in HSV-2 subunit vaccines? *Expert Rev. Vaccines* 13: 691–710.
54. Banatvala, J. E., and P. Van Damme. 2003. Hepatitis B vaccine – do we need boosters? *J. Viral Hepat.* 10: 1–6.
55. Hazlett, L. D., P. Wells, and R. S. Berk. 1981. Immunocytochemical localization of IgA in the mouse cornea. *Exp. Eye Res.* 32: 97–104.
56. Allansmith, M., A. de Ramus, and D. Maurice. 1979. The dynamics of IgG in the cornea. *Invest. Ophthalmol. Vis. Sci.* 18: 947–955.
57. Osusky, R., A. Morell, P. Imbach, and P. G. Lerch. 1993. Diffusion of immunoglobulins into rabbit cornea after subconjunctival injection: experimental demonstration and mathematical model. *Graefes Arch. Clin. Exp. Ophthalmol.* 231: 122–128.
58. Gipson, I. K. 2007. The ocular surface: the challenge to enable and protect vision: the Friedenwald lecture. *Invest. Ophthalmol. Vis. Sci.* 48: 4390; 4391–4398.
59. Akpek, E. K., and J. D. Gottsch. 2003. Immune defense at the ocular surface. *Eye (Lond.)* 17: 949–956.
60. Knop, E., and N. Knop. 2005. The role of eye-associated lymphoid tissue in corneal immune protection. *J. Anat.* 206: 271–285.
61. Hazlett, L. D., and R. S. Berk. 1989. Kinetics of immunoglobulin appearance at the ocular surface. *Reg. Immunol.* 2: 294–299.
62. Masinick, S. A., C. P. Montgomery, P. C. Montgomery, and L. D. Hazlett. 1997. Secretory IgA inhibits *Pseudomonas aeruginosa* binding to cornea and protects against keratitis. *Invest. Ophthalmol. Vis. Sci.* 38: 910–918.
63. Friedman, M. G., and N. Kimmel. 1982. Herpes simplex virus-specific serum immunoglobulin a: detection in patients with primary or recurrent herpes infections and in healthy adults. *Infect. Immun.* 37: 374–377.
64. Ashley, R. L., F. M. Crisostomo, M. Doss, R. E. Sekulovich, R. L. Burke, M. Shaughnessy, L. Corey, N. L. Polissar, and A. G. Langenberg. 1998. Cervical antibody responses to a herpes simplex virus type 2 glycoprotein subunit vaccine. *J. Infect. Dis.* 178: 1–7.
65. Petro, C., P. A. González, N. Cheshenko, T. Jandl, N. Khajouejad, A. Bénard, M. Sengupta, B. C. Herold, and W. R. Jacobs. 2015. Herpes simplex type 2 virus deleted in glycoprotein D protects against vaginal, skin and neural disease. *eLife* 4: e06054.
66. Karring, H., I. B. Thøgersen, G. K. Klintworth, T. Møller-Pedersen, and J. J. Enghild. 2006. The human cornea proteome: bioinformatic analyses indicate import of plasma proteins into the cornea. *Mol. Vis.* 12: 451–460.
67. Maurice, D. M., and P. G. Watson. 1965. The distribution and movement of serum albumin in the cornea. *Exp. Eye Res.* 4: 355–363.
68. Chaudhry, C., C. L. Brooks, D. C. Carter, J. M. Robinson, and C. L. Anderson. 2006. Albumin binding to FcRn: distinct from the FcRn-IgG interaction. *Biochemistry* 45: 4983–4990.
69. Dickinson, B. L., K. Badizadegan, Z. Wu, J. C. Ahouse, X. Zhu, N. E. Simister, R. S. Blumberg, and W. I. Lencer. 1999. Bidirectional FcRn-dependent IgG transport in a polarized human intestinal epithelial cell line. *J. Clin. Invest.* 104: 903–911.
70. Waldrep, J. C., R. L. Noe, and R. D. Stulting. 1988. Analysis of human corneal IgG by isoelectric focusing. *Invest. Ophthalmol. Vis. Sci.* 29: 1538–1543.
71. Bai, Y., L. Ye, D. B. Tesar, H. Song, D. Zhao, P. J. Björkman, D. C. Roopenian, and X. Zhu. 2011. Intracellular neutralization of viral infection in polarized epithelial cells by neonatal Fc receptor (FcRn)-mediated IgG transport. *Proc. Natl. Acad. Sci. USA* 108: 18406–18411.
72. Li, Z., S. Palaniyandi, R. Zeng, W. Tuo, D. C. Roopenian, and X. Zhu. 2011. Transfer of IgG in the female genital tract by MHC class I-related neonatal Fc receptor (FcRn) confers protective immunity to vaginal infection. *Proc. Natl. Acad. Sci. USA* 108: 4388–4393.
73. Liszewski, M. K., M. Elvington, H. S. Kulkarni, and J. P. Atkinson. 2017. Complement's hidden arsenal: New insights and novel functions inside the cell. *Mol. Immunol.* 84: 2–9.
74. Kolev, M., G. Le Fric, and C. Kemper. 2014. Complement-tapping into new sites and effector systems. *Nat. Rev. Immunol.* 14: 811–820.
75. Tam, J. C., S. R. Bidgood, W. A. McEwan, and L. C. James. 2014. Intracellular sensing of complement C3 activates cell autonomous immunity. *Science* 345: 1256070.
76. Elvington, M., M. K. Liszewski, P. Bertram, H. S. Kulkarni, and J. P. Atkinson. 2017. A C3(H2O) recycling pathway is a component of the intracellular complement system. *J. Clin. Invest.* 127: 970–981.
77. Kolev, M., and C. Kemper. 2017. Keeping it all going-complement meets metabolism. *Front. Immunol.* 8: 1.
78. Da Costa, X. J., M. A. Brockman, E. Alicot, M. Ma, M. B. Fischer, X. Zhou, D. M. Knipe, and M. C. Carroll. 1999. Humoral response to herpes simplex virus is complement-dependent. *Proc. Natl. Acad. Sci. USA* 96: 12708–12712.
79. Verschoor, A., M. A. Brockman, M. Gadjeva, D. M. Knipe, and M. C. Carroll. 2003. Myeloid C3 determines induction of humoral responses to peripheral herpes simplex virus infection. *J. Immunol.* 171: 5363–5371.
80. Awasthi, S., J. M. Lubinski, and H. M. Friedman. 2009. Immunization with HSV-1 glycoprotein C prevents immune evasion from complement and enhances the efficacy of an HSV-1 glycoprotein D subunit vaccine. *Vaccine* 27: 6845–6853.
81. Lubinski, J. M., H. M. Lazear, S. Awasthi, F. Wang, and H. M. Friedman. 2011. The herpes simplex virus 1 IgG Fc receptor blocks antibody-mediated complement activation and antibody-dependent cellular cytotoxicity in vivo. *J. Virol.* 85: 3239–3249.
82. Lubinski, J., L. Wang, D. Mastellos, A. Sahu, J. D. Lambris, and H. M. Friedman. 1999. In vivo role of complement-interacting domains of herpes simplex virus type 1 glycoprotein gC. *J. Exp. Med.* 190: 1637–1646.
83. Petro, C. D., B. Weinrick, N. Khajouejad, C. Burn, R. Sellers, W. R. Jacobs, and B. C. Herold. 2016. HSV-2 Δ gD elicits Fc γ R-effector antibodies that protect against clinical isolates. *JCI Insight* 1: e88529.
84. Mallery, D. L., W. A. McEwan, S. R. Bidgood, G. J. Towers, C. M. Johnson, and L. C. James. 2010. Antibodies mediate intracellular immunity through tripartite motif-containing 21 (TRIM21). *Proc. Natl. Acad. Sci. USA* 107: 19985–19990.
85. Liu, X., L. Ye, G. J. Christianson, J.-Q. Yang, D. C. Roopenian, and X. Zhu. 2007. NF- κ B signaling regulates functional expression of the MHC class I-related neonatal Fc receptor for IgG via intronic binding sequences. *J. Immunol.* 179: 2999–3011.
86. Liu, X., L. Ye, Y. Bai, H. Mojidi, N. E. Simister, and X. Zhu. 2008. Activation of the JAK/STAT-1 signaling pathway by IFN- γ can down-regulate functional expression of the MHC class I-related neonatal Fc receptor for IgG. *J. Immunol.* 181: 449–463.
87. Lewis, G. K., A. L. DeVico, and R. C. Gallo. 2014. Antibody persistence and T-cell balance: two key factors confronting HIV vaccine development. *Proc. Natl. Acad. Sci. USA* 111: 15614–15621.

Table S1. Invitrogen Silencer Select siRNAs

Target	Catalog # / siRNA ID	Antisense siRNA sequence
Scramble control	4390843	Negative control #1 (undisclosed)
Mu. FCGRT (FcRn)	4390771 / s65924	5'-UUGACAUUGAUAAUGGUGCtc-3'
Mu. FCGRT (FcRn)	4390771 / s65926	5'-UCCCAUUUAAUAUCUUCUCca-3'

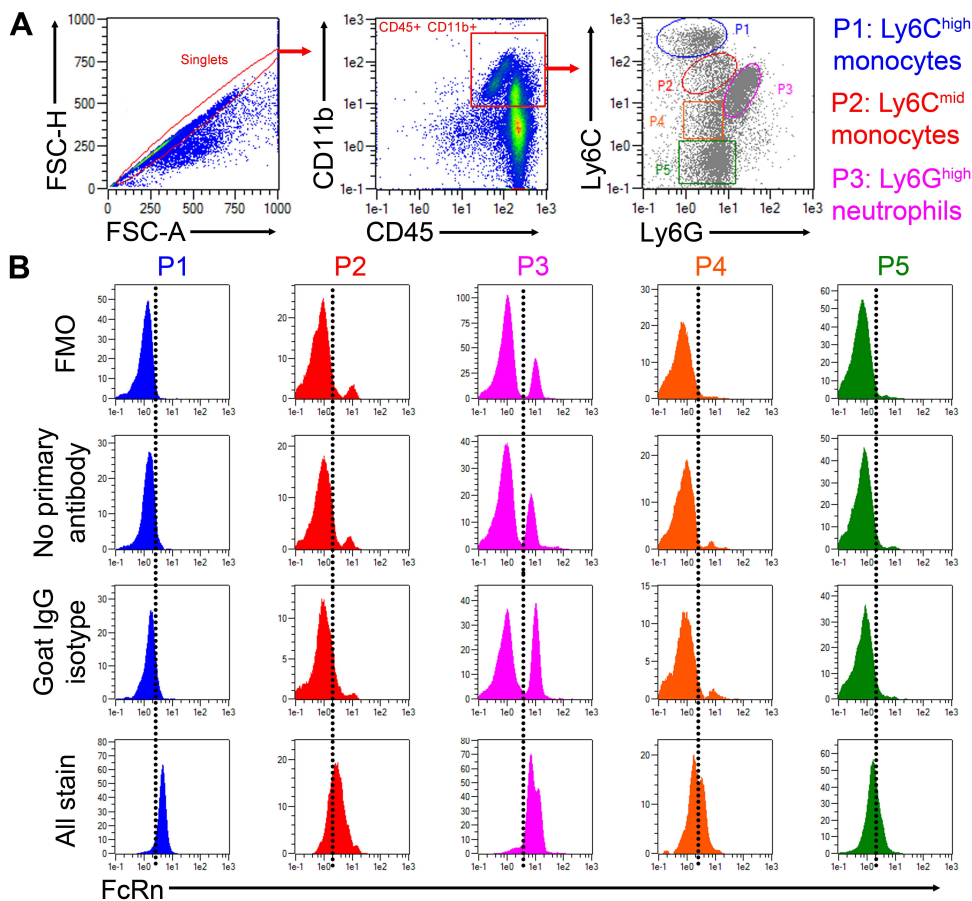
Abbreviations: FCGRT, Fc fragment of IgG receptor and transporter; FcRn, neonatal Fc receptor; Mu., murine. Lowercase letters in sequence denote mutated nucleotide bases.

Supplemental Figure 1 (Related to Figure 6)



Supplemental Figure 1 (Related to Figure 6): Antibody perfusion in vascularized nerve ganglia and skin. (A) Concentrations of immunoglobulin by isotype in the trigeminal ganglia (TG) as in Fig. 6A (n = 6-8 individual TG/group; 2-3 independent experiments). (B) Concentration of immunoglobulin by isotype in the healthy or hole-punched ear pinna (24 hours post-injury) to evaluate dynamics of antibody perfusion in a vascularized, non-mucosal site (n = 6 pinna samples/group; 2 independent experiments). Statistical differences were determined by one-way ANOVA with Student-Newman-Keuls multiple comparisons tests for panel A or Student's T test for panel B.

Supplemental Figure 2 (Related to Figure 8)



Supplemental Figure 2 (Related to Figure 8): Colocalization of HSV-1 and C3d. (A) Flow cytometry was used to assess subpopulations of circulating CD45⁺ CD11b⁺ myeloid cells using Ly6C and Ly6G antigens in peripheral blood. (B) Analysis of FcRn expression by MFI (median fluorescence intensity) in subsets defined in panel A. Controls are shown on the left margin.

Supplemental Movie 1 (Related to Figure 7): 3D profile C3d accumulation in the corneal epithelium of vaccinated.

Animation provides multi-dimensional perspectives of intracellular C3d (red) deposition in the cornea as described in Figure 7. Tissue was counterstained with phalloidin (green) to label F-actin and delineate cellular boundaries. Mixed model renderings of threshold-adjusted z-stack image data and isosurface projections are shown. Animation was created using Imaris software (Bitplane, Zurich, Switzerland).